# Buckling Behavior of U-Shaped Girders

**by**

**Christopher Lee Gilchrist, B.S.C.E.**

**Thesis**

Presented to the Faculty of the Graduate School of

The University of Texas at Austin

in Partial Fulfillment

of the Requirements

for the Degree of

**Master of Science in Engineering**

**The University of Texas at Austin**

**May, 1997**

**Buckling Behavior of U-Shaped Girders**

Approved by
Supervising Committee:

Joseph A. Yura

Karl H. Frank

*To my family*

## Acknowledgements

The author would like to thank Dr. Joseph Yura for his patience, encouragement, and guidance throughout the course of this research. His insight and positive outlook made this research a terrific learning experience. Thanks also go to Dr. Karl Frank and Dr. Todd Helwig for their ideas and comments.

The author is especially indebted to Reagan Herman. This research and thesis would not have been completed without her daily support, ideas, humor, encouragement, and manual labor.

The author would also like to acknowledge the staff at the Phil M. Ferguson Structural Engineering Laboratory for their support during this project. Special thanks go to Mike Bell for all of his efforts during the creation of the experimental test setup. Thanks also go to Sharon Cunningham for her assistance with the writing of this thesis.

Thanks go to all of the students at Ferguson Laboratory who helped in the development of this research. The friends who have aided in this work are too many to list on one page. You know who you are. Special thanks go to Mike Gilroy for encouraging me to get a job and re-introducing me to the game of ping-pong. Thanks also go to Kristin Grubbs for her care and support.

Finally, the author wishes to acknowledge the Texas Department of Transportation for their funding of this research project.

March 14, 1997

# Buckling Behavior of U-Shaped Girders

Christopher Lee Gilchrist, M.S.E

The University of Texas at Austin, 1997

Supervisor: Joseph A. Yura

Trapezoidal box girder systems are becoming a popular form of curved bridge system because of their torsional stiffness and aesthetic appearance. The systems typically consist of twin steel U-shaped girders with a concrete deck acting compositely as the top flange. The top flanges of these U-girders are susceptible to lateral-torsional buckling during transport, erection, and placement of the deck. There is no existing codified design method for bracing of U-shaped girders. Minimizing the amount of bracing used will lead to a more efficient design since this bracing makes up a significant amount of the total costs and is not utilized once the concrete deck has cured.

In order to develop a design procedure for lateral bracing of U-girders, the behavior of unbraced U-shaped girders was first studied. An analytical program was undertaken to study the buckling behavior of unstiffened and transversely stiffened U-shaped girders using finite element models. A series of laboratory experiments were then performed using U-girder scale models in order to verify these analytical results. Finally, the analytical and experimental results were compared with existing design equations for torsionally braced I-shaped beams.

# TABLE OF CONTENTS

# LIST OF TABLES

# LIST OF FIGURES

# CHAPTER 1

# Introduction

## 1.1 DESCRIPTION

The use of trapezoidal box girder systems for curved bridges is becoming increasingly popular because of their torsional stiffness and aesthetic appearance. A typical system consists of two steel U-shaped girders placed side-by-side with a concrete deck acting compositely as the top flange, as shown in Figure 1.1.

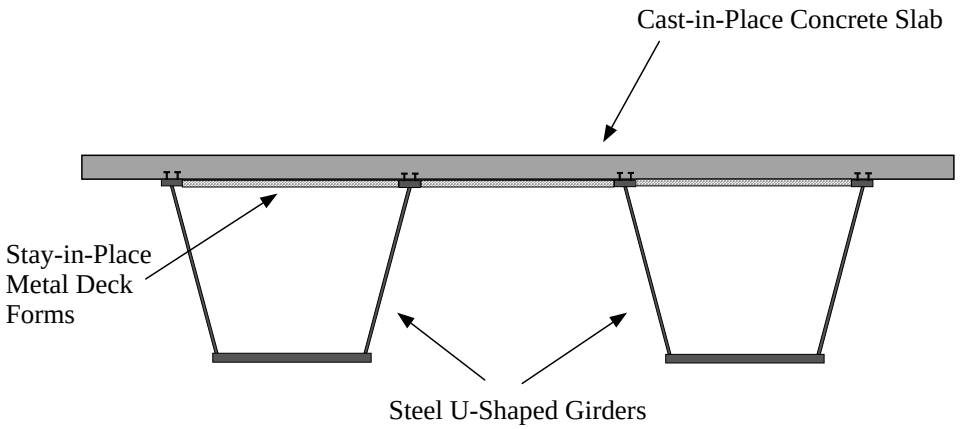


***Figure 1.1: Cross-Section of Trapezoidal Box Girder System***

Construction of trapezoidal box girder systems occurs in several stages. The U-shaped girders are assembled at a fabrication shop. The flange and web plates are cut and welded together using various jigs and automated welding equipment. The girders are fabricated in segments typically 40-120 ft in length for ease of transport to the job site. Figure 1.2 shows several U-girder segments

prior to erection. Segments are spliced together after they are lifted into place using bolted splice plates. The erected U-girders are shown in Figure 1.3. After the U-shaped girders are bolted together, stay-in-place metal deck forms are placed between the flanges of the two girders. A reinforced concrete slab is then poured in stages along the length of the bridge to control girder stress and conrete shrinkage. After curing, the deck acts compositely with the U-girders through shear studs on the top flanges. A completed trapezoidal box girder bridge is shown in Figure 1.4.

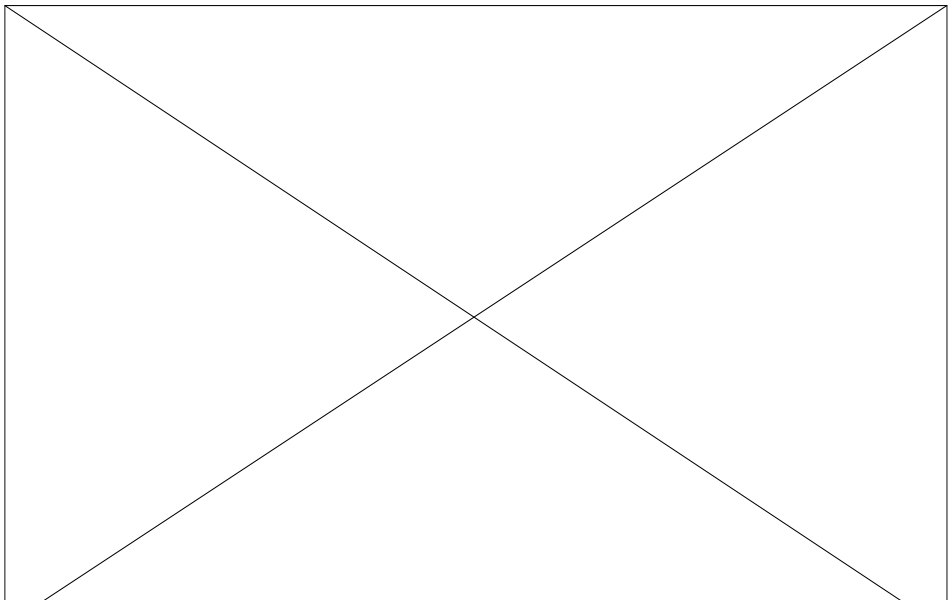

***Figure 1.2: U-Shaped Girders Prior to Erection***

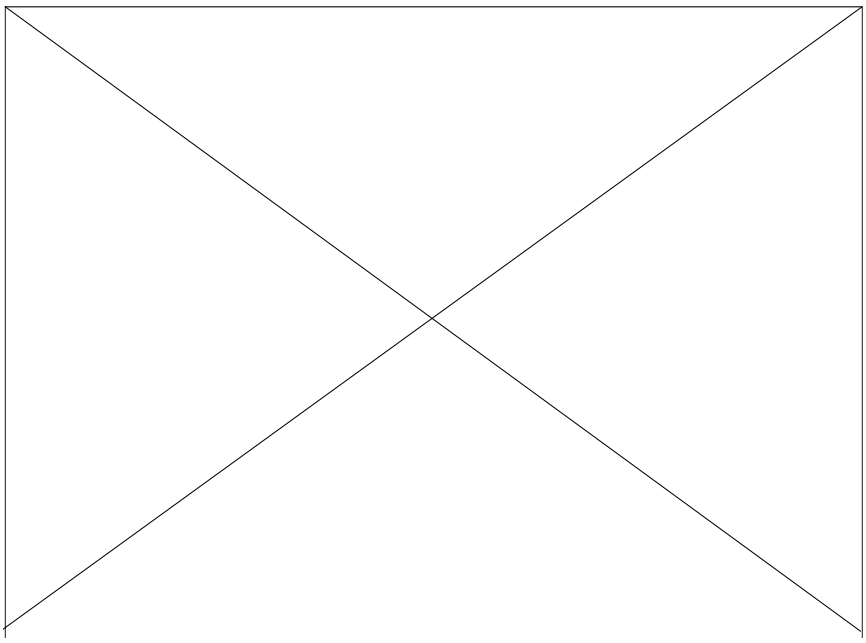

***Figure 1.3: U-Shaped Girders During Erection in Houston, TX***

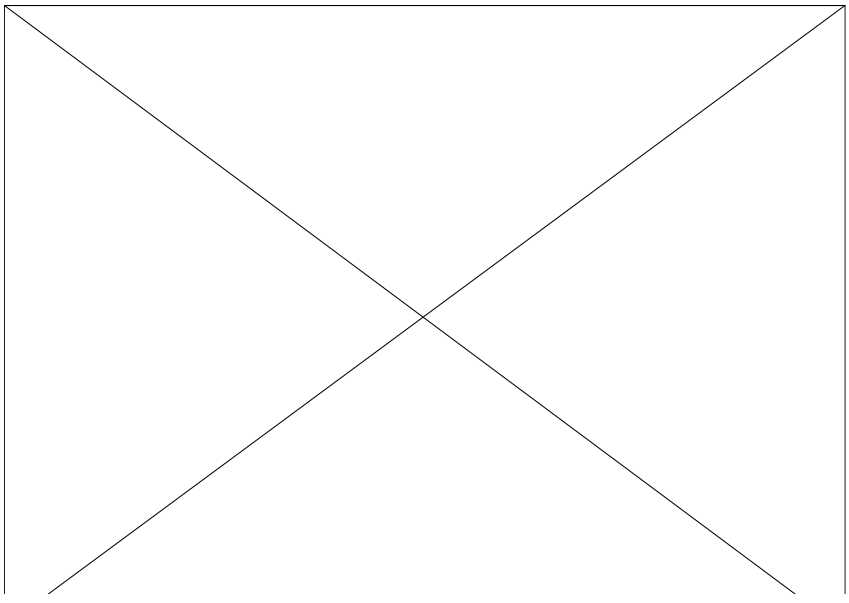

***Figure 1.4: Erected U-Shaped Girders Prior to Deck Placement***

The concrete deck placed on top of the U-girders creates two closed trapezoidal boxes. These closed boxes provide a path for shear flow around the cross-section, dramatically increasing the torsional rigidity of the system. Figure 1.5 shows the shear flow resulting from an applied eccentric load. A closed cross-section can often have a torsional stiffness several thousand times that of a similar open section (Basler, 1969).

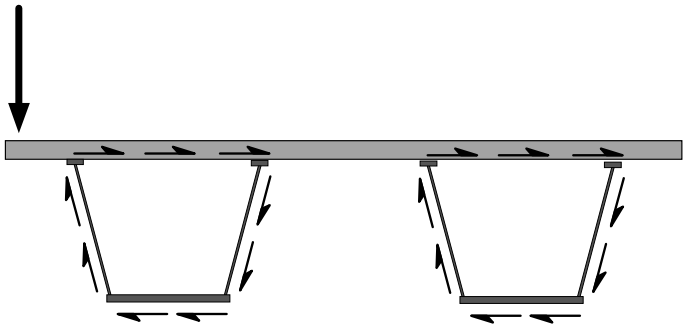

***Figure 1.5: Shear Flow Resulting from Eccentric Load***

## 1.2 NEED FOR U-GIRDER BRACING

The steel U-shaped girders feature narrow top flanges, especially in the positive bending sections of the bridge where the composite concrete deck is in compression. In these positive moment areas, the width of the steel section's top flange is typically dictated only by the number of shear studs necessary for composite behavior since the top flange is near the neutral axis. Prior to curing of the deck, the neutral axis of the steel girder is closer to the bottom flange. At this stage the top flanges are in compression and are susceptible to lateral-torsional

buckling. Lateral bracing of these flanges is necessary to avoid buckling from loads encountered during transport, erection, and deck placement.

Before the concrete deck cures, the U-shaped girders act as open sections and their torsional stiffness is small. To resist the large torsional moments which occur when construction gravity loads are applied to the curved girders, lateral bracing between the top flanges is needed to effectively close the cross-section and provide a path for shear flow.

Once the concrete deck has cured, the bridge acts as a composite section. The deck provides continuous lateral bracing for the top flanges and also closes the cross-section of each U-girder. Thus, the lateral and torsional bracing placed in the U-girders for construction loadings is no longer required after the concrete has hardened.

## 1.3 TYPES OF BRACES

There are several types of braces used for U-shaped girders. This bracing, which is placed on the interior of the girder, is typically designed to increase the girder's resistance to torsional moments and concentrated forces. As a secondary effect, these braces provide lateral support for the top flanges and thus increase the buckling strength of the girder.

### 1.3.1 Top Lateral Systems

One type of bracing used in U-shaped girders is a top lateral system. Top lateral bracing consists of a horizontal truss system near the plane of the top

flanges running the entire length of the girder, as shown in Figure 1.6. A top lateral system can also be seen in Figures 1.3 and 1.4.

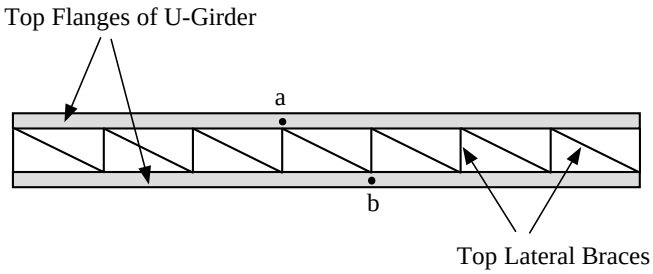


***Figure 1.6: Top Lateral Bracing System***

The function of this lateral system is two-fold. First, it connects the top flanges of the girder and creates a path for shear flow around the cross-section. This creates a psuedo-closed cross-section that has a much larger torsional stiffness than the an unbraced section. The other effect of the top lateral braces is to increase the buckling strength of the U-girder by providing lateral bracing along the top flanges. This bracing prevents differential lateral movement of the top flanges at points connected by the bracing (points A and B of Figure 1.6). Therefore lateral buckling cannot occur except between the brace points. A design approach for relative lateral bracing of I-shaped girders has been developed by Yura (1993).

### 1.3.2 Diaphragms

Interior diaphragms can also provide bracing in U-shaped girders. These diaphragms are typically either K-shaped cross-frames or solid plates, as shown in

Figure 1.7, which are placed at various points along the length of the girder. The solid plates are usually located at support points where the piers apply concentrated forces to the girders. These diaphragm plates prevent local crippling and cross-section distortion. The K-shaped cross-frames are typically spaced at regular intervals along the girder's length. They are used to prevent cross-section distortion that results from torsional moments in the curved girder. This cross-section distortion is illustrated in Figure 1.8.

Interior diaphragms can add to the lateral buckling strength of the girder by preventing local distortion of the cross-section. However, a diaphragm located at a point where no cross-section distortion occurs (i.e. a node point in the buckled shape) has no effect on the girder's buckling strength.

### 1.3.3 Web Stiffeners

Transverse stiffeners are attached to the webs of the U-shaped girders, as shown in Figure 1.9, to increase their shear strength. They typically run the full height of the web and are attached with welds to the web and bottom flange. These stiffeners add to the buckling strength of the U-girder by increasing the lateral bending stiffness of the web.

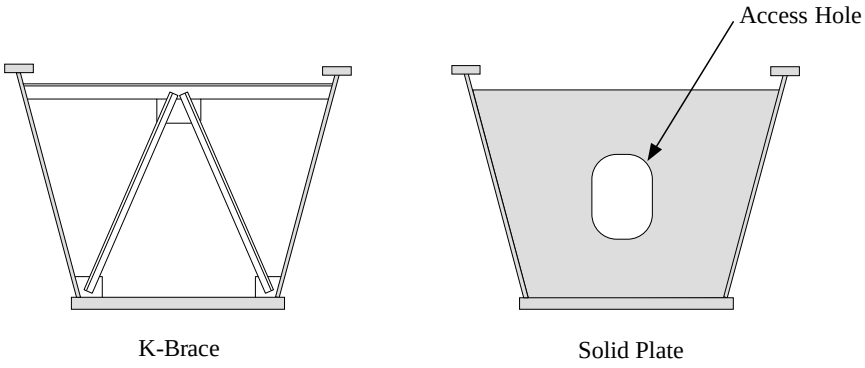


***Figure 1.7: Interior U-Girder Diaphragms and Stiffeners***

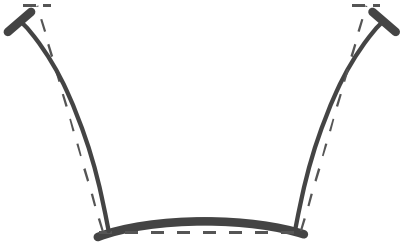

***Figure 1.8: Cross-Section Distortion***

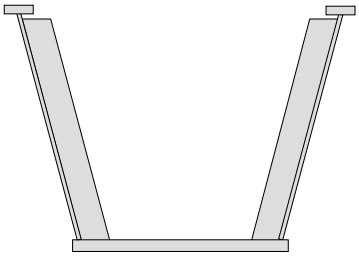

***Figure 1.9: Web Stiffeners***

## 1.4 CURRENT LATERAL BRACING DESIGN REQUIREMENTS

The current AASHTO (American Association of State Highway and Transportation Officials) *Guide Specifications for Horizontally Curved Highway Bridges* provides very limited information on the lateral bracing requirements for the top flanges of steel box girders. Section 10.6 of the specification states:

> *These girders shall have diagonal top flange bracing to cause the steel section to act as a pseudo closed section. Diagonal top flange bracing shall be adequate to resist torsion applied to the steel section prior to the deck curing. Top flanges shall be assumed braced at points where interior bracing is located.*

Winter (1960) has shown that a lateral brace must have adequate strength and stiffness to act as an effective brace point. The current AASHTO specification provides no strength or stiffness requirements for lateral braces of U-shaped girders. There is no existing design method for lateral bracing of U-shaped girders.

## 1.4 OBJECTIVES OF RESEARCH

The work presented in this paper is part of research project 1395, "Trapezoidal Box Girder Systems", sponsored by the Texas Department of Transportation. This four year research project will investigate the design and behavior of box girder systems and includes analytical, experimental, and field

studies. The box girder bridge pictured in Figures 1.2-1.4 was instrumented prior to construction and is part of an ongoing field study.

The aim of this portion of the project is to determine the minimum bracing required to resist construction loads for U-shaped girders. The current specifications provide no means for determining the bracing necessary to resist lateral-torsional buckling or torsional loading. It is important to minimize the bracing placed in U-shaped girders since this bracing is not utilized after the concrete deck of the box girder system has cured. Currently, the material and fabrication costs of the lateral bracing system make up a significant amount of the total box girder costs. For example, top lateral bracing used in the center span of the Houston, TX bridge shown previously increased the weight of the girders by almost 12%. By reducing the amount of bracing for U-shaped girders, trapezoidal box girders can become a more efficient and cost effective bridge system.

The design of the top lateral bracing system should consider not only the torsional stiffness of the U-girder, but also the lateral buckling strength necessary to resist construction loadings. In order to develop bracing requirements for the lateral buckling strength, it is first necessary to understand the buckling behavior of the unbraced U-shaped girder. The objectives of this report are to:

1. Study the buckling behavior of unstiffened and transversely stiffened U-shaped girders analytically using finite element models.
2. Verify the analytical results experimentally with scale models of U-shaped girders.

3. Compare the analytical and experimental results with design equations for braced I-shaped girders.

Using the results of this study, the buckling strength of U-shaped girders with top flange lateral bracing can then be addressed. These studies will lead to minimum requirements and design procedures for lateral bracing of U-shaped girders.

Chapter 2 of this thesis presents an analytical study of U-shaped girder buckling behavior. Chapter 3 describes an experimental program which was completed, and the results of this program are presented in Chapter 4. A comparison of the analytical and experimental results is included in Chapter 5, with conclusions presented in Chapter 6.

# CHAPTER 2

# Analytical Program

## 2.1 GENERAL

An analytical program was undertaken to study the buckling behavior of U-shaped girders under uniform moment conditions. Based on existing torsional bracing theory, a simplified U-girder finite element model was first developed to isolate factors affecting buckling behavior. A more complete U-girder finite element model was then created to verify the simple model and study the differences between rectangular and trapezoidal cross-sectional shapes. These models were also used to design test specimens for use in the experimental test program. Finally, the analytical results were compared with existing design equations for beams with continuous torsional bracing.

The buckling behavior of a U-shaped girder can be understood by considering the girder as two separate "half-girders" with a connecting bottom flange. The wide bottom flange adds restraint to the half-girders in two ways. First, if either girder is to twist as buckling occurs, the bottom flange must bend as illustrated in Figure 2.1. Thus the bottom flange adds restraint which can be idealized as a torsional brace running continuously along the length of the girder. The stiffness of the continuous brace varies depending on whether the half-girders rotate in the same direction or opposite directions, also shown in Figure 2.1. Second, if the bottom of the girder is to move laterally, the bottom flange must

bend about the weak axis of the girder. However, the lateral moment of inertia of the bottom flange is so large that practically no lateral movement will occur. This can be idealized on the half-girder as a continuous, infinite lateral restraint attached to the bottom flange as shown in Figure 2.2. To obtain the buckling load for a complete U-girder, the buckling load of the half-girder is doubled.

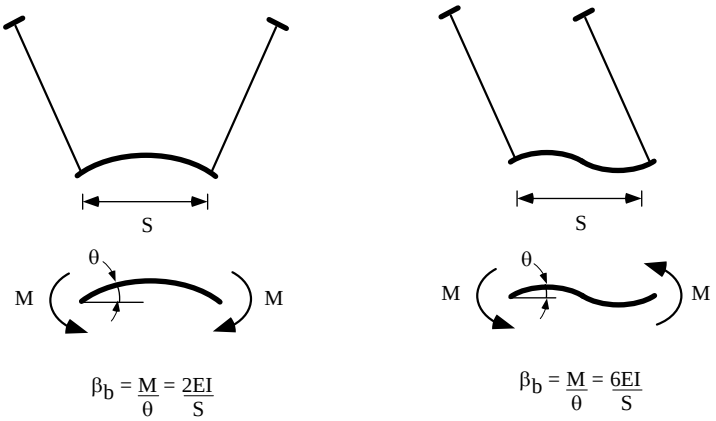


***Figure 2.1 : Torsional Restraint of Bottom Flange***

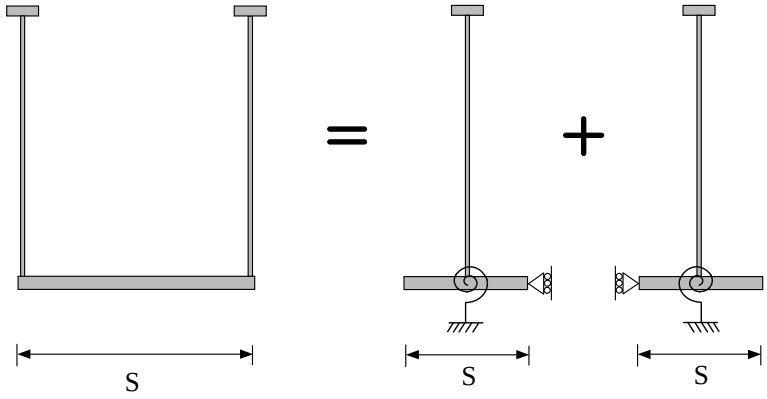


***Figure 2.2 : Half-Girder Model of Box Girder***

## 2.2 BUCKLING STRENGTH OF TORSIONALLY BRACED BEAMS

The critical moment of a doubly symmetric beam under uniform moment with continuous torsional bracing (Taylor and Ojalvo, 1973) is:

$$M_{cr} = \sqrt{M_0 + \bar{\beta}_b EI_y} \tag{1}$$

where $M_0$ is the buckling capacity of the unbraced beam, $\bar{\beta}_b$ is the continuous torsional brace stiffness (e.g. k-in/rad per inch of girder length), E is the elastic modulus of the material, and $I_y$ is the beam's out-of-plane moment of inertia. Equation (1) assumes that the cross-section of the beam does not distort during buckling. The results from Equation (1) are shown in Figure 2.3 by the dot-dash line. Cross-section distortion causes poor correlation between Equation (1) and results provided by Yura (1992) using the finite element program BASP (Akay, 1977; Choo, 1987). The distortion occurs when the web bends laterally and can be accounted for by using an effective brace stiffness, $\bar{\beta}_T$, which was developed by Milner (1977) and expanded (Yura, 1992) to include the effect of stiffeners :

$$\frac{1}{\bar{\beta}_T} = \frac{1}{\bar{\beta}_b} + \frac{1}{\bar{\beta}_{sec}} \tag{2}$$

where $\bar{\beta}_b$ is the stiffness of the torsional brace, and $\bar{\beta}_{sec}$ is the cross-section web stiffness. Equation (2) states that the total stiffness of the brace must less that the smallest of $\bar{\beta}_b$ and $\bar{\beta}_{sec}$. The value of $\bar{\beta}_b$ for half of a U-shaped girder depends on the relative rotation of the two half-girders, as shown in Figure 2.1.

The effects of cross-section distortion can be approximated (Yura, 1993) by considering the flexibility of the web, including full depth stiffeners if any, using the following equation :

$$\bar{\beta}_{sec} = 3.3\frac{E}{h}\left(\frac{{t_w}^3}{12} + \frac{n t_s {b_s}^3}{12L}\right) \tag{3}$$

where $t_w$ = thickness of the web, h = depth of web, $t_s$ = thickness of stiffener, n = number of stiffeners, L = length of girder, and $b_s$ = width of stiffener, as shown in Figure 2.4. Using Equation (3) to account for cross-section distortion gives answers almost identical to the BASP solutions, as shown by the dashed lines in Figure 2.3.

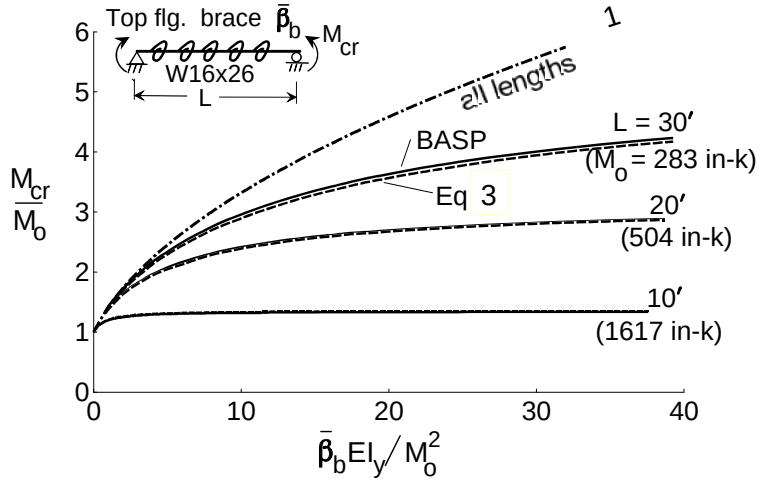


***Figure 2.3 : Torsionally Braced Buckling Formula***

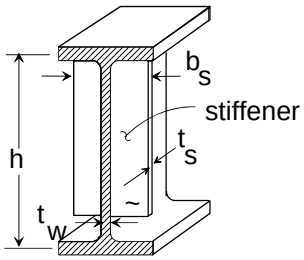

***Figure 2.4 : Dimensions of Full Depth Web Stiffener***

Equation (1) was developed for beams with doubly-symmetric cross-sections. Yura (1993) determined that the torsional bracing effect for singly-symmetric sections can be approximated by replacing $I_y$ in Equation (1) with an effective moment of inertia $I_{eff}$ defined as :

$$I_{eff} = I_{yc} + \frac{t}{c} I_{yt} \tag{4}$$

where $I_{yc}$ and $I_{yt}$ are the lateral moment of inertia of the compression flange and tension flange respectively, and c and t are the distances from the neutral bending axis to the centroid of the compression and tension flanges respectively, as shown in Figure 2.5(a). This equation was developed for cross-sections where the ratio $I_{yc}/I_y$ is greater than 0.1 and less than 0.9.

By adjusting for cross-section distortion and singly-symmetric cross-sections, the following formula can be used for the buckling strength of beams with continuous torsional bracing:

$$M_{cr} = \sqrt{M_0 + \bar{\beta}_T \, EI_{eff}} \leq M_y \tag{5}$$

where $\bar{\beta}_T$ is the effective continuous torsional brace stiffness (k-in/rad per inch length) from Equation (2) and $I_{eff}$ is the effective moment of inertia from Equation (4). Equation (5) indicates that the buckling load increases without limit as the effective brace $\bar{\beta}_T$ increases, or until the yield moment of the section $M_y$ is reached. Figure 2.5(b) provides a comparison between BASP solutions and Equation (5) for three different singly-symmetric girders with torsional braces. In

each case the equations are in close agreement with the theoretical buckling load given by BASP.

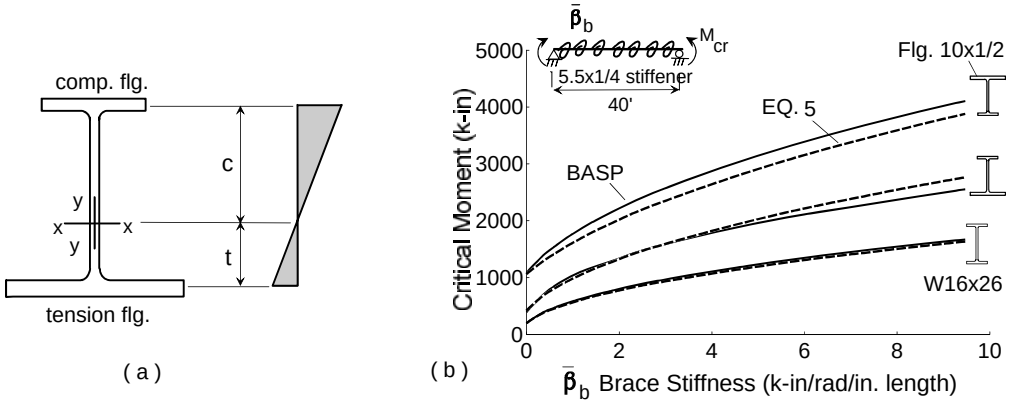


***Figure 2.5 : Singly-Symmetric Girders***

The torsionally braced beam solution given by Equation (5) may not be directly applicable to U-girders because the bottom flange is laterally braced. In addition, the dimensions of the girders of interest to this research have $I_{yc}/I_y$ ratios less than 0.1, which are outside the limits studied in the development of Equation (5). Therefore, a more detailed buckling analysis was performed as described in the following sections.

## 2.3 U-GIRDER BUCKLING BEHAVIOR

The buckling behavior of U-shaped girders was studied using the half-girder model described previously. Finite element models of half-girders were studied using the computer program BASP.

### 2.3.1 Description of BASP Computer Program

The finite element program BASP, an acronym for "buckling analysis of stiffened plates", was developed at The University of Texas at Austin by Akay (1977) and modified for use on a personal computer by Choo (1987). BASP is a two-dimensional finite element program that gives eigenvalue buckling modes for stiffened I-shaped beams and T-sections. Many types of restraints may be modeled, including torsional springs at any node point. The program is limited to elastic modeling of initially straight beams with loads applied only in the plane of the web. BASP does account for web distortion and was used in the development of the design equations discussed in Section 2.2.

A BASP model was created based on the half-girder analogy presented in Section 2.1. Since the analytical results were to be compared with experiments, the support and loading conditions were modeled in a way which would be easy to simulate in the laboratory. The boundary conditions for the BASP model are shown in Figure 2.6. The model consisted of a girder 40 ft. in length, with simple supports located six feet from each end. Load was applied at each end of the girder, creating a 28 ft. center span where the girder was subjected to uniform moment. Out-of-plane boundary conditions, including lateral restraints and rotational springs, were based on the half-girder model shown in Figure 2.2. Rotational springs were placed at each node along the bottom flange, and their stiffness was calculated based on the thickness of the bottom flange, the width of the flange, and the spacing of the nodes along the length of the girder. A lateral restraint was provided at each node along the bottom flange, preventing bottom

flange lateral movement. In addition, top flange lateral restraints were provided at the support and load points of the girder.

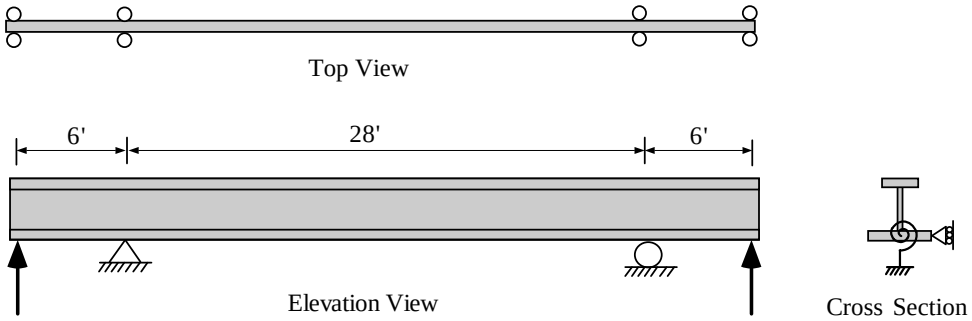


***Figure 2.6 : Boundary Conditions for BASP Model***

The cross-section dimensions of the half-girder model shown in Figure 2.7 were selected based on several considerations. First, the dimensions should be proportional to actual U-girders used in bridges. Dimensions of an actual bridge being constructed in Houston, Texas were checked to ensure similar proportions. The cross-section selected was roughly one-quarter the size of actual U-girders used in this bridge. Second, the girders should buckle elastically, with the yield moment $M_y$ of the girder significantly higher than the buckling load. This would make it possible during the experimental program to perform numerous laboratory tests on the same test specimen. Third, the experimental phase of the study would require U-girders small enough to be tested in the laboratory. The cross-section shown in Figure 2.7 was determined to best satisfy these criteria, based on a series of trial designs modeled with BASP. These dimensions were used for all BASP models presented in this chapter and correspond closely with the actual

dimensions of the laboratory specimens used in the experimental program described in Chapter 3.

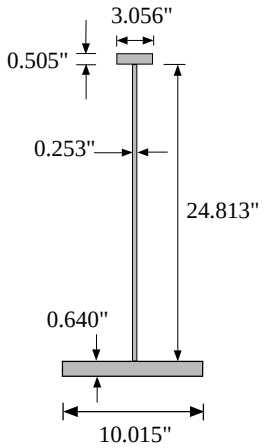


***Figure 2.7 : Cross-Section Dimensions of BASP Model***

### 2.3.2 Effects of Increasing Torsional Brace Stiffness

As mentioned previously, the wide bottom flange of the U-girder can be considered to act as a continuous torsional brace attached to the bottom flange of each half-girder. The stiffness of this torsional brace is dependent upon the thickness and width of the bottom flange.

Using BASP, the buckling behavior of an unstiffened half-girder with continuous torsional bracing was studied. By varying the stiffness of the torsional springs in BASP, the bottom flange's torsional bracing effect could be isolated without change to any cross-section properties of the half-girder. The results of this study are shown in Figure 2.8.

As the brace stiffness is increased, the buckling load increases non-linearly. With no bracing, the half-girder's top flange buckles into one wave. With just 1.67 k-in/rad/in of torsional bracing, the top flange buckles into two

waves. For a U-girder with a 20 inch wide bottom flange, this would correspond to a bottom flange thickness of 0.19 inches based on a 2EI/S stiffness. Beyond 50 k-in/rad/in, increasing the torsional brace stiffness has almost no effect on the buckling load. This is due to cross-section distortion of the web. For this unstiffened half-girder, a continuous torsional brace can increase the buckling capacity about 100% above the torsionally unbraced case.

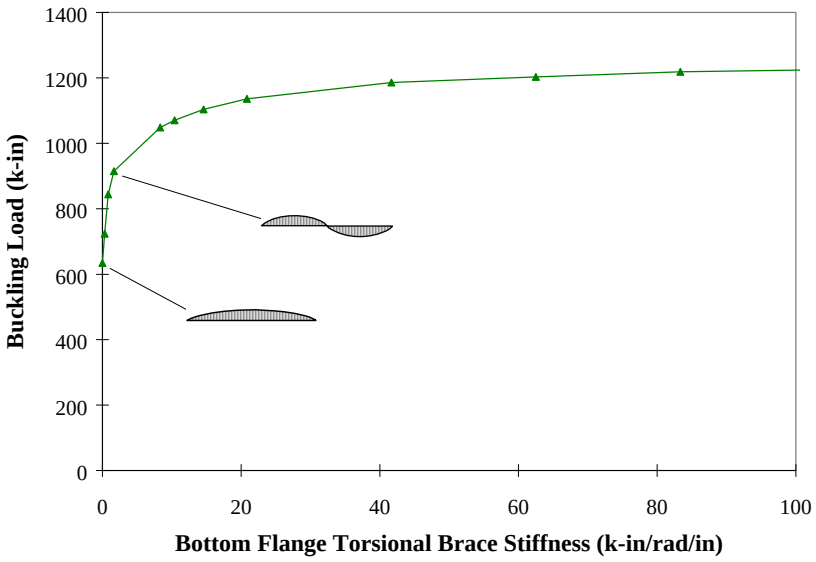


***Figure 2.8 : Effects of Increasing Torsional Brace Stiffness***

### 2.3.3 Effects of Cross-Section Distortion

Yura (1993) has shown that even small amounts of web distortion can have significant effects on the buckling load of torsionally braced beams. Equation (2) indicates that the effectiveness of a torsional brace is limited by the stiffness of the web, $\bar{\beta}_{sec}$. However, distortion can be controlled through the use of web stiffeners, as indicated in Equation (3).

Figure 2.9 illustrates the effects of cross-section distortion. By placing eight 4 in. x 0.1 in. stiffeners spaced equally along the length of the half-girder, distortion is greatly reduced and the buckling load increases to almost twice that of the girder with the unstiffened web. This corresponds to approximately four times the unbraced girder buckling load. Eliminating cross-section distortion allows higher buckling modes to be attained. The top flange buckles into 3 waves at a torsional stiffness of 1560 k-in/rad/in and 4 waves at 2440 k-in/rad/in.

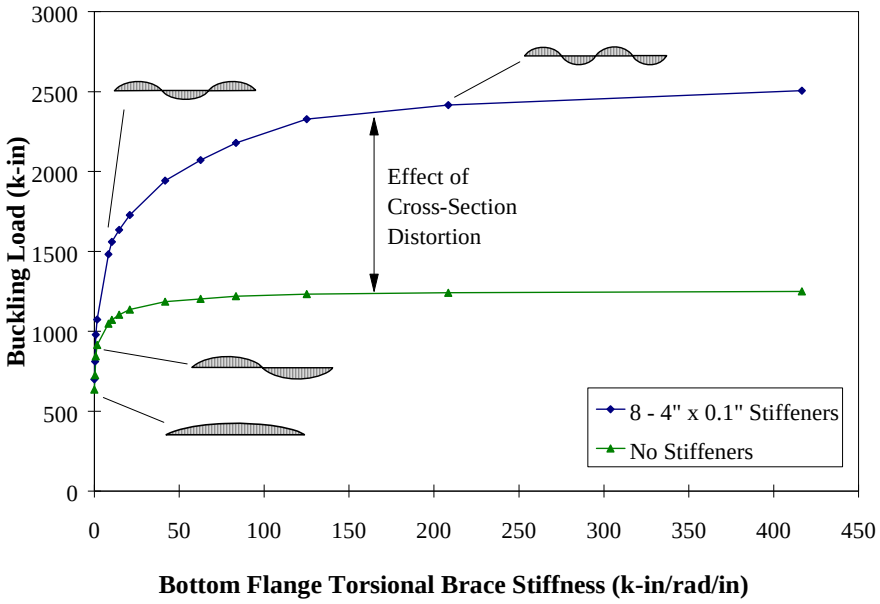


***Figure 2.9 : Effect of Cross-Section Distortion on Buckling Load***

### 2.3.4 Effects of Continuous Lateral Bracing

As discussed in Section 2.1, the wide bottom flange of a U-girder has such a large lateral moment of inertia that it acts similar to a continuous lateral brace.

Yura (1993) shows that the position of a lateral brace has a very significant effect on the buckling strength of a beam, with the most effective lateral brace located at the top flange. A lateral brace located along the tension flange has very little effect on the buckling strength of a beam. Figure 2.10 shows BASP results verifying that a lateral brace along the bottom flange of the half-girder model has almost no effect on the buckling load.

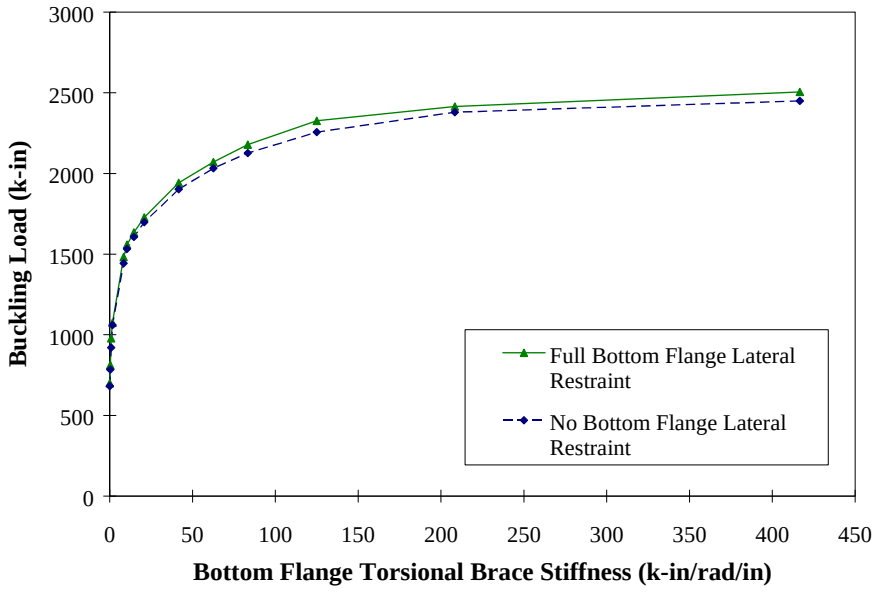


***Figure 2.10 : Effect of Continuous Bottom Flange Lateral Brace***

## 2.4 FINITE ELEMENT MODELS OF U-GIRDERS

A more comprehensive U-girder model was developed to verify the half-girder analogy and study the differences in behavior of rectangular and

trapezoidal cross-sectional shapes since the BASP program cannot model trapezoidal sections.

A finite element model of the U-girder presented in Figure 2.2 was created using the program ABAQUS. ABAQUS is a commercial finite element package developed by Hibbitt, Karlsson & Sorensen, Inc.. It is capable of numerous analysis types, including eigenvalue and large displacement analyses. The U-girder model created for this study was composed of 8-noded shell elements, ABAQUS type S8R. These elements are designed for modeling of thin plates and have a two-dimensional geometry, with the thickness of the plate being entered as a material property of the element.

Boundary conditions for the ABAQUS model were similar to those used in the BASP study. There were no lateral restraints provided along the bottom flange since the whole U-girder was modeled. Each top flange was restrained laterally at the ends and at the support locations, 6 ft. from each end. Vertical loads were applied at the mid-height of each of the webs at both ends.

Two models were created, one with a rectangular cross-section and the other with a trapezoidal cross-section. The finite element models are shown in Figure 2.11. Both the girders had the same size flanges and the depths of the two girders were equal. This allowed for a direct comparison of buckling load between the two girders, isolating the effects of the sloping webs. The cross-section properties of the two models are given in Figure 2.12. Eigenvalue buckling modes were extracted for each of the U-girder models.

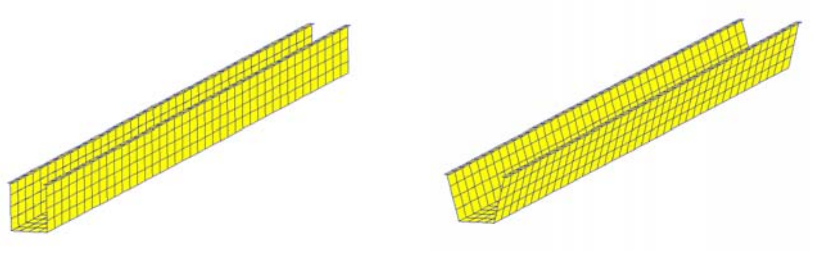

(a) (b)

***Figure 2.11 : Finite Element Models of the (a) Rectangular and (b) Trapezoidal U-girders***

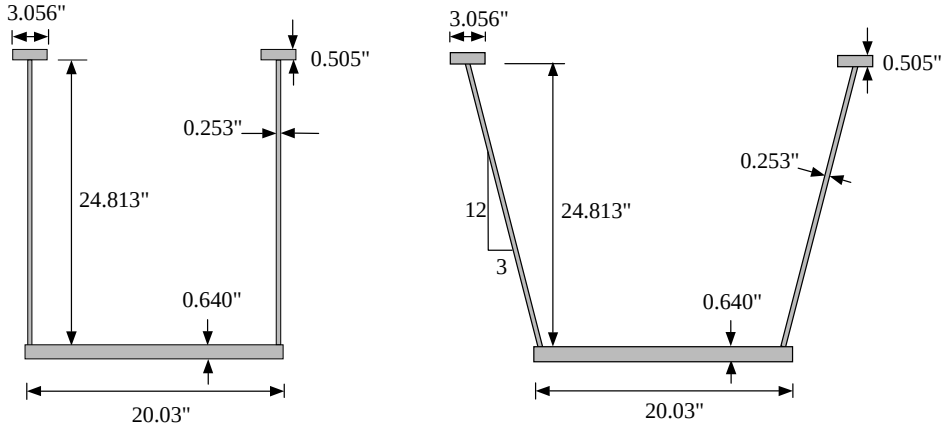


A = 28.46 $in^2$

Ix = 2676 $in^4$

$Sx_{top}$ = 155.0 $in^3$

A = 28.83 $in^2$

Ix = 2696 $in^4$

$Sx_{top}$ = 160.9 $in^3$

***Figure 2.12 : Cross-Section Properties of U-Girder Finite Element Models***

### 2.4.1 Rectangular Girder Eigenvalue Results

Plan views of the rectangular U-girder showing the first six eigenvalue buckling modes are provided in Figure 2.13. The girder's uniform moment region

is located between the lateral supports as shown in Figure 2.13. The first six eigenvalues are listed in Table 2.1. In the first buckling mode, both flanges buckle into two waves between the supports. The two flanges rotate in opposite directions at all points along the length of the girder, which corresponds with the bottom flange bending in single curvature.

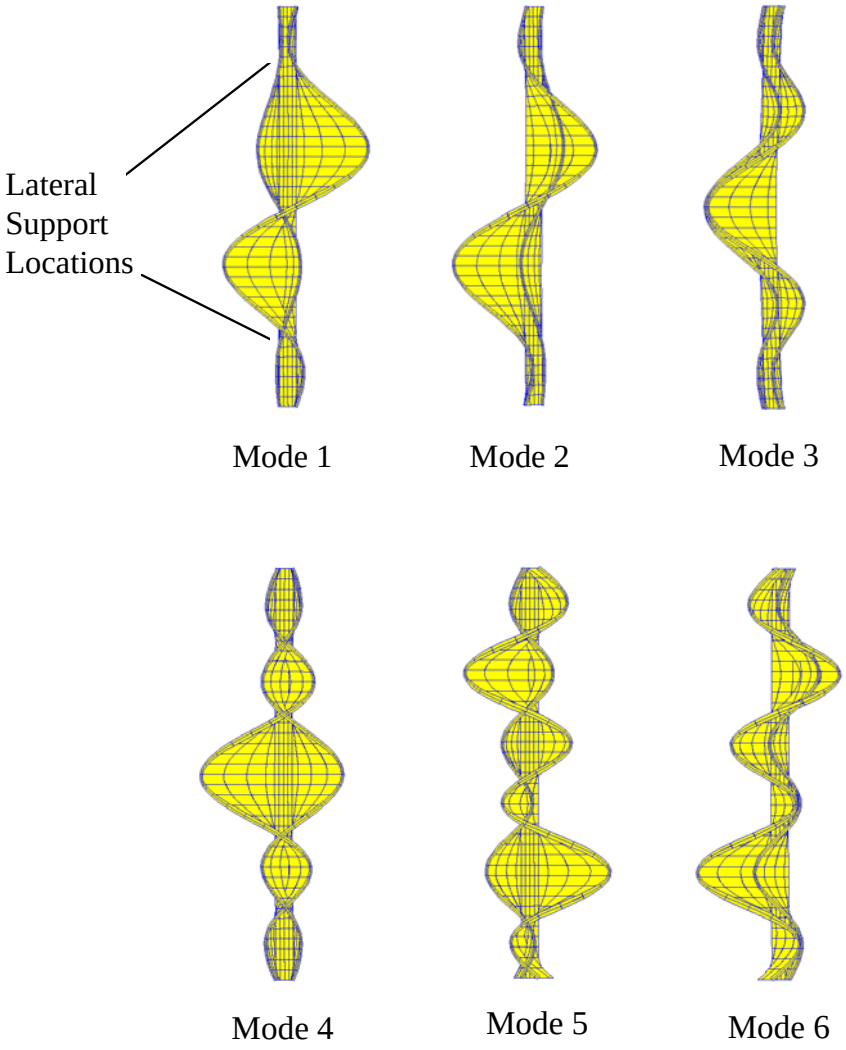


***Figure 2.13 : First Six Buckling Modes for Rectangular U-Girder***

***Table 2.1 : First Six Eigenvalues of Rectangular U-Girder***

| Eigenvalue Number | Eigenvalue (k-in) | Number of Top Flange Waves Between Supports | Percent Greater than First Eigenvalue |
|---|---|---|---|
| 1 | 2706 | 2 | --- |
| 2 | 2718 | 2 | 0.5 % |
| 3 | 2879 | 3 | 6.4% |
| 4 | 2889 | 3 | 6.8 % |
| 5 | 3859 | 4 | 42.6 % |
| 6 | 3902 | 4 | 44.2 % |

The second buckling mode is similar to the first, except the flanges rotate in the same direction corresponding with the bottom flange bending in double curvature, with a bending stiffness of 6EI/S. This stiffness is three times the stiffness of a plate bending in single curvature, so this mode requires more energy and would be expected occur at a higher load than the bottom flange single curvature bending. However, the difference between the first and second modes is just 0.5%, which can be explained by examining a cross-section of the buckled shape shown in Figure 2.14. Because the bottom plate is much stiffer than the webs, almost all of the distortion occurs in the webs, with very little bending of the bottom flange. Thus, cross-section distortion is very significant for U-girder buckling.

Table 2.1 shows that there are pairs of eigenvalues that have similar values, with larger differences between the pairs. Each group of two eigenvalues

corresponds to a certain number of waves of the top flange, with the first pair of eigenvalues (1 and 2) having two waves, followed by three waves for the next pair, then four. The lower eigenvalue of the pair corresponds with the flanges rotating in opposite directions (a 2EI/S bottom flange stiffness), and the higher eigenvalue with the flanges rotating in the same direction (6EI/S stiffness).

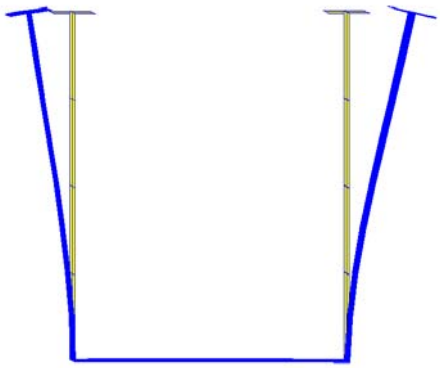

***Figure 2.14 : Cross-Section of Buckled Shape of Rectangular U-Girder***

The half-girder model was compared with the rectangular U-girder analysis to verify the analogy of the bottom flange acting as a continuous torsional brace. , A continuous torsional spring with stiffness of 61.04 k-in/rad/in was input into the BASP model. The spring stiffness was calculated based on the dimensions of the bottom flange and assuming single curvature bending with stiffness 2EI/S. This resulted in a two wave buckled shape with a buckling load of 2720.7 k-in, or just 0.5% difference from the ABAQUS results.

### 2.4.2 Trapezoidal Girder Eigenvalue Results

Eigenvalue buckling modes for the U-girder with a trapezoidal cross-section are shown in Figure 2.15. The eigenvalues corresponding to these shapes are provided in Table 2.2.

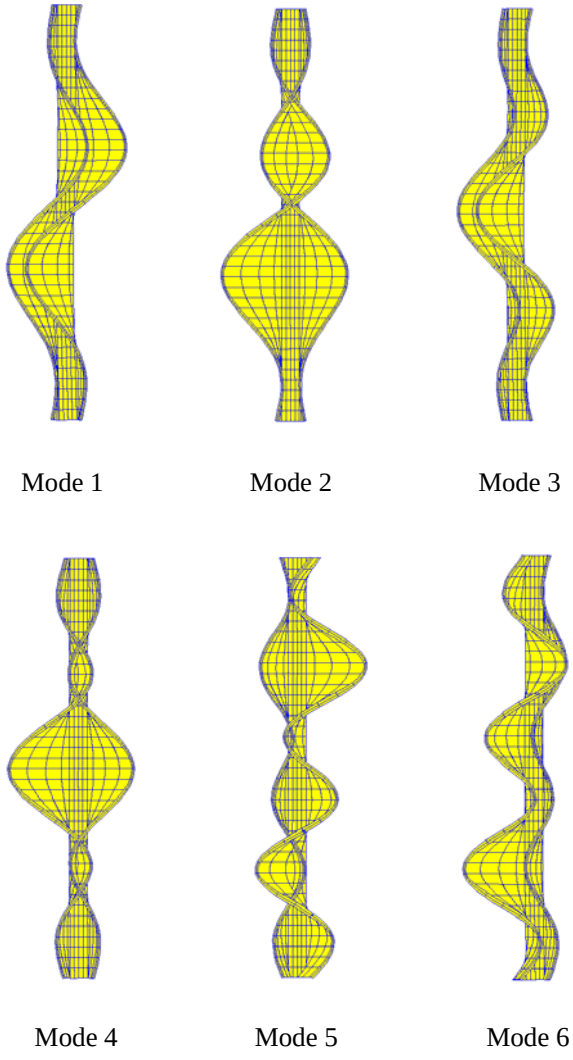


***Figure 2.15 : First Six Buckling Modes for Trapezoidal U-Girder***

***Table 2.2 : First Six Eigenvalues of Trapezoidal U-Girder***

| Eigenvalue Number | Eigenvalue (k-in) | Percent Greater than First Eigenvalue | Percent Less than Corresponding Rectangular Girder Eigenvalues |
|---|---|---|---|
| 1 | 2492 | --- | 8.5 % |
| 2 | 2520 | 1.1 % | 7.9 % |
| 3 | 2670 | 7.1 % | 7.8 % |
| 4 | 2701 | 8.4 % | 7.0 % |
| 5 | 3607 | 44.7 % | 7.0 % |
| 6 | 3642 | 46.1 % | 7.1 % |

There are several notable differences in the eigenvalue results for the rectangular and trapezoidal U-girders. First, the trapezoidal girder has an eigenvalue buckling load 8.5% less than that of the rectangular girder. Second, the first buckling mode for the trapezoidal girder features the top flanges displacing in the same direction, with the flanges displacing in opposite directions in the second mode. This is the reverse of the rectangular girder's first two buckling modes.

The trapezoidal girder's lower buckling load and reversed buckling modes can be explained by studying the effects of the inclined webs. When the top flanges of the girder displace in opposite directions, the bottom flange bends in single curvature as shown in Figure 2.1. The free-body diagram of the bottom flange shows that the moments M are in equilibrium. When the top flanges displace in the same direction, the bottom flange is bent into double curvature and

the moments both have the same direction. For the bottom flange to be in equilibrium, shear forces occur as shown in Figure 2.16 and are transferred to the webs. The effects of these shear forces on the buckling strength of torsionally braced twin girders have been investigated by Helwig (1993). Shear transferred to an inclined web has both a vertical and horizontal component. As shown in Figure 2.16, the horizontal components of shear for a trapezoidal girder act in the same direction. These extra lateral forces result in a lower buckling load for the case where the top flanges displace in the same direction. Since the critical moments of the first two buckling modes are so close, this extra lateral force may be enough to cause the bottom flange double-curvature mode to occur first.

The trapezoidal U-girders studied for this report were all loaded with uniform moment. Shear occurring because of non-uniform moment conditions will also have horizontal components and may affect the buckling loads of U-girders with inclined webs.

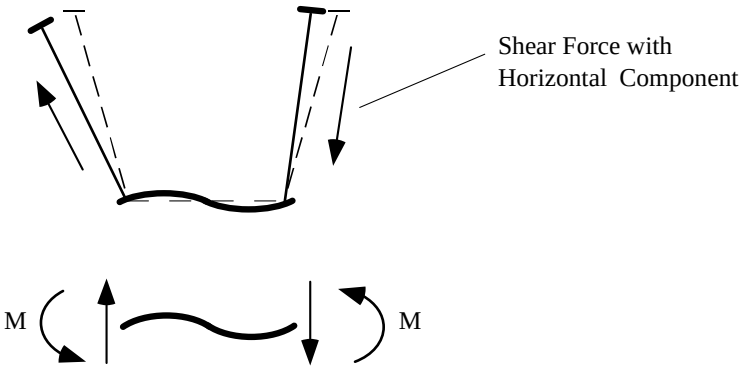


***Figure 2.16: Shear Resulting from Double-Curvature of Bottom Flange for Trapezoidal Girder***

### 2.4.3 Effects of Stiffeners

Figure 2.14 shows that cross-section distortion plays a large part in the buckling of U-shaped girders. As stated previously, the buckling strength of any torsionally braced beam can be significantly reduced by even a small amount cross-section distortion. One way to increase the buckling capacity of U-shaped girders is to decrease this distortion using web stiffeners.

The ABAQUS rectangular U-girder model presented above was modified to include web stiffeners. A series of analyses were performed with varying numbers and sizes of stiffeners. The stiffeners extended over the full height of the web and were attached rigidly at the bottom to a stiffening plate of equal height and thickness across the bottom flange. These three plates were connected together to form a U-shaped frame which was attached to the outside of the girder. The bottom stiffener was included to ensure that the angle between the webs and bottom flange was maintained. The stiffeners are shown in Figure 2.17.

Two configurations of stiffeners were analyzed. The first configuration consisted of stiffeners attached at the first and third quarter-points of the center span. The second configuration featured stiffeners attached to all three quarter-points of the center span. The two configurations are shown in Figure 2.17.

For each configuration, two different sizes of stiffeners were compared. This resulted in a total of four different stiffener combinations for the rectangular U-girder finite element model. The eigenvalue results from the four analyses are listed in Table 2.3. The buckled shapes corresponding with these eigenvalues are shown in Figure 2.18.

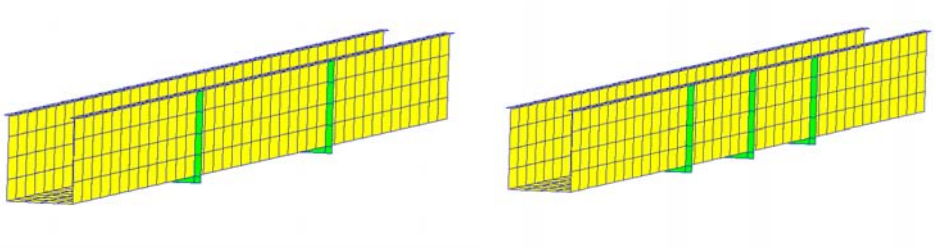

***Figure 2.17 : Two Stiffener Configurations Analyzed***

2” x 0.285” Stiffeners
1st, 3rd Quarter Pts.

2” x 0.285” Stiffeners
1st, 2nd, 3rd Quarter Pts.

2” x 1.635” Stiffeners
1st, 3rd Quarter Pts.

2” x 1.635” Stiffeners
1st, 2nd, 3rd Quarter Pts.

***Figure 2.18 : Buckled Shapes for Stiffened Rectangular U-Girders***

***Table 2.3 : Eigenvalue Analysis Results for Stiffened Rectangular U-Girders***

| Stiffener Size (in) | Stiffener Location (quarter pt) | Eigenvalue Buckling Load (k-in) | Number of Waves in Top Flanges | Percent Difference from Unstiffened Case |
|---|---|---|---|---|
| Unstiffened | --- | 2706 | 2 | --- |
| 2 x 0.285 | 1st and 3rd | 2936 | 3 | 8.5 % |
| 2 x 1.635 | 1st and 3rd | 3058 | 3 | 13.0 % |
| 2 x 0.285 | 1st, 2nd, 3rd | 3704 | 4 | 36.9 % |
| 2 x 1.635 | 1st, 2nd, 3rd | 4497 | 4 | 66.2 % |

## 2.5 COMPARISON OF FINITE ELEMENT RESULTS WITH CONTINUOUS TORSIONAL BRACING EQUATIONS

The buckling capacity of the unstiffened rectangular U-girder was calculated using the continuous torsional bracing equations presented in Section 2.2. These calculations were based on the half-girder cross-section presented in Figure 2.7. The calculated values were compared with results from BASP and ABAQUS finite element models.

The boundary conditions assumed were equivalent to those presented previously, with a 28 ft simple span under uniform moment. The bottom flange torsional brace stiffness $\bar{\beta}_b$ was calculated to be 65.5 k-in/rad/in, assuming a stifffness of 2EI/S for single curvature bending of the bottom flange. Using Equation (3) with no web stiffeners, the cross-section stiffness term $\bar{\beta}_{sec}$ was determined to be 5.38 k-in/rad/in. The combination of these two stiffnesses using

Equation (2) gives an effective torsional brace stiffness $\bar{\beta}_T$ = 4.975 k-in/rad/in. Thus the more flexible web reduces the effectiveness of the bottom flange torsional brace by over 92%. This provides an illustration of the dramatic effects of cross-section distortion.

The effective moment of inertia $I_{eff}$ was calculated to be 28.2 $in^4$. The unbraced buckling strength of the girder $M_0$ was determined using the AISC LRFD equations for singly-symmetric beams found in Appendix F, Table A-F1.1. Based on the cross-section properties of the half-girder, $M_0$ was calculated to be 580.9 k-in. This value compares closely with the BASP result for the unbraced case shown in Figure 2.8. The BASP result is slightly higher because of the warping restraint caused by the endspans of the finite element model.

The buckling load for this half-girder was then calculated using Equation (5), resulting in an $M_{cr}$ of 2130.8 k-in for the half-girder. To determine the buckling load for the entire U-girder this load was then multiplied by two, giving an $M_{cr}$ of 4261.6 k-in. This result is 58% greater than the buckling load calculated using BASP.

The cause of this discrepancy is the effective moment of inertia term, $I_{eff}$. The $I_{eff}$ approximation was developed for unsymmetrical sections where the ratio of $I_{yc}/I_y$, also known as $\rho$, is between 0.1 and 0.9. As shown in Figure 2.5(b), it gives very good results for unsymmetrical cross-sections within these $\rho$ limits. However, for this half-girder $\rho$ is just 0.02. It is apparent form the results above that using the $I_{eff}$ term for cross-sections with small $\rho$ values can give very unconservative results.

# CHAPTER 3

# Experimental Program

## 3.1 GENERAL

The experimental program consisted of laboratory tests designed to study the buckling behavior of U-shaped girders and the effects of various bracing configurations. Two model U-shaped girders were fabricated. The first girder was a rectangular girder consisting of one bottom flange and two top flanges connected with vertical webs. The second girder had identical flanges but featured sloping webs, giving it a trapezoidal shape.

The girders were simply supported with overhanging end spans. Each girder was 40 ft. in length with a 28 ft. center span and 6 ft. overhangs on each end, as shown in Figure 3.1 The girders were loaded at the ends to achieve a uniform bending moment region between the supports. Figure 3.2 shows the overall test setup.

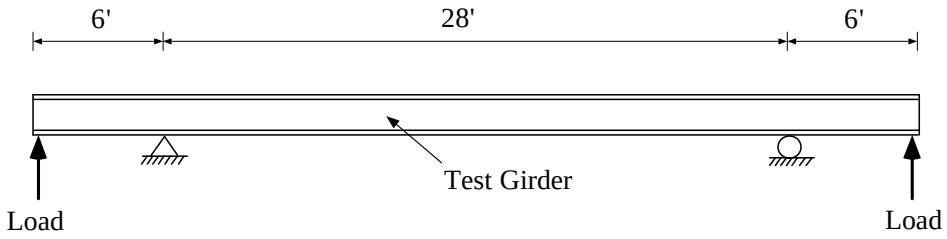


***Figure 3.1: Schematic of Test Setup***

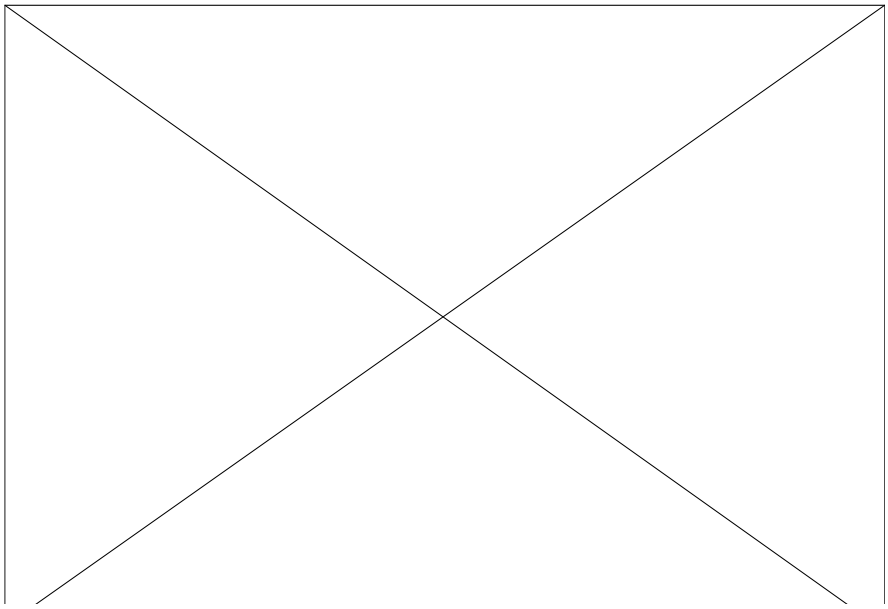

***Figure 3.2: Overall Test Setup***

### 3.2 TEST SPECIMENS

The two box-girders used in the testing program were designed to buckle elastically when unbraced and with a variety of bracing schemes, based on BASP and ABAQUS finite element analyses. The girders were fabricated using steel with a nominal yield strength of 50 ksi for the top and bottom flanges, and 36 ksi for the webs.

The girders were originally designed to have identical strong axis cross-sectional properties. However, an error in the fabrication of the girders resulted in the rectangular girder having a depth 1.54 inches greater than the trapezoidal specimen. Both girders had cross-sectional dimensions approximately one-quarter of the size of U-shaped girders used in the bridge shown in Figure 1.2 to 1.4, located in Houston, Texas. The web slope of the trapezoidal specimen was

identical to that of the Houston bridge girder. The average measured cross-sectional properties of the rectangular and trapezoidal girders are provided in Figures 3.3 and 3.4, respectively.

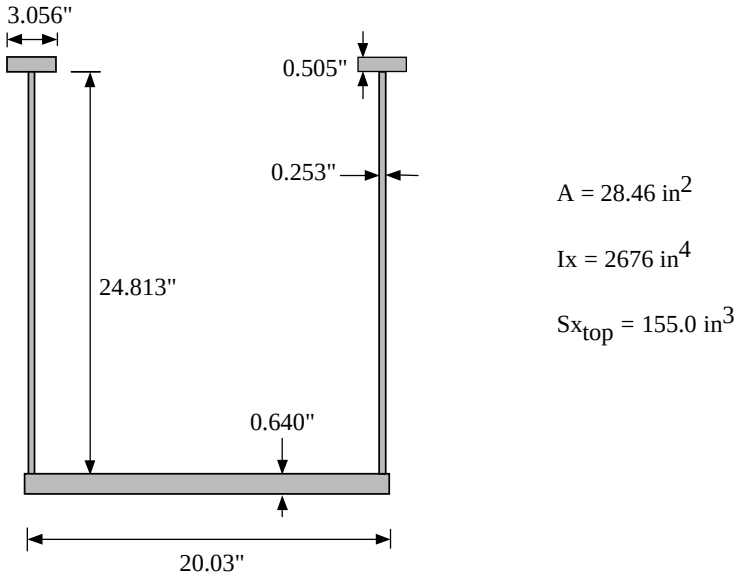


***Figure 3.3: Cross-Sectional Properties of Rectangular Girder***

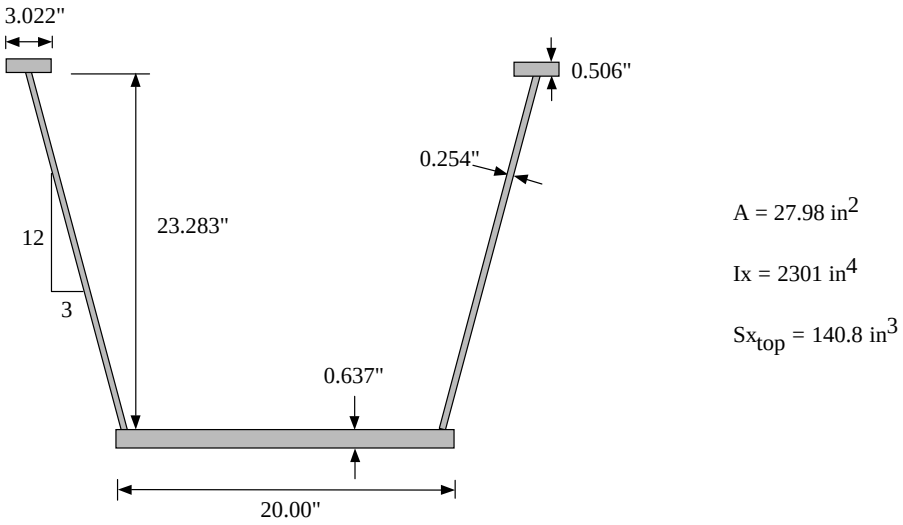


***Figure 3.4: Cross-Sectional Properties of Trapezoidal Girder***

### 3.3 LOADING AND SUPPORT SYSTEMS

A support system was designed for the tests to approximate a simply supported condition. The supports consisted of 24 inch long W36 x 150 beams oriented in a direction transverse to the direction of the box-girder as shown in Figure 3.5. The bottom flange of the support beam was bolted to the floor using four 1 in. diameter rods. The top flange of the support beam was bolted to the bottom flange of the girder using four 1 in. diameter bolts.

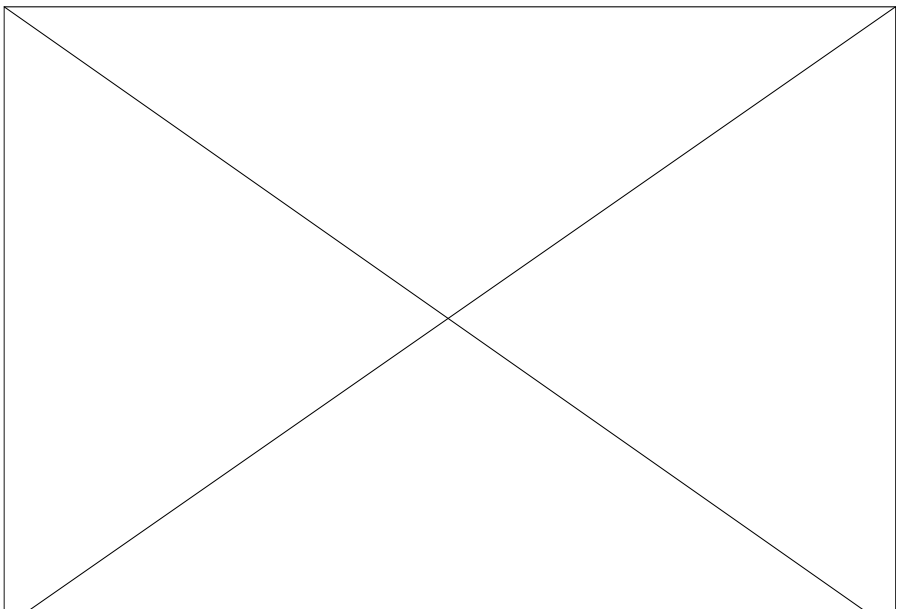

***Figure 3.5: Support Beam***

The support beams approximated a pinned condition since the bending resistance of the webs provided little rotational restraint while limiting movement laterally. The rotational restraint caused by the supports can be conservatively estimated as 4EI/L by considering the web of the support beam as rigidly attached to the floor. Thus the rotational stiffness provided by the support is 1824 k-in./rad based on the support dimensions. At the yield moment $M_y$ of the box-girder, the support would provide a restraining moment of 37.7 k-in., or just 1.3 % of $M_y$.

Load was applied to the bottom flange of the specimen 4.5 inches from the ends of the girder using hydraulic rams. The rams were both connected to a single hand pump, ensuring that equal loads would be applied simultaneously at the two load points. A roller/bearing assembly was placed between the ram and the girder to assure that the line of action of the load would remain vertical even

after the endspans began to deflect. A load cell was placed beneath each of the rams to measure the load as it was applied. For spacing purposes a 1 in. thick steel plate was placed between the floor and the load. The loading assembly is shown in Figure 3.6.

Permanent cross frames were installed at the support locations and the ends of the girder to prevent lateral movement of the top flanges at these locations. The support cross frames consisted of two 3 in. x 2 in. x 1/4 in. angles as shown in Figure 3.7. The angles were attached at the top to a 3 in. x 3/8 in. plate connecting the two webs. At the bottom the angles were attached to a WT 7 x 26.5, which was bolted through the girder to the top flange of the support beam. All angles and plates were welded in place with 1/4 in. welds.

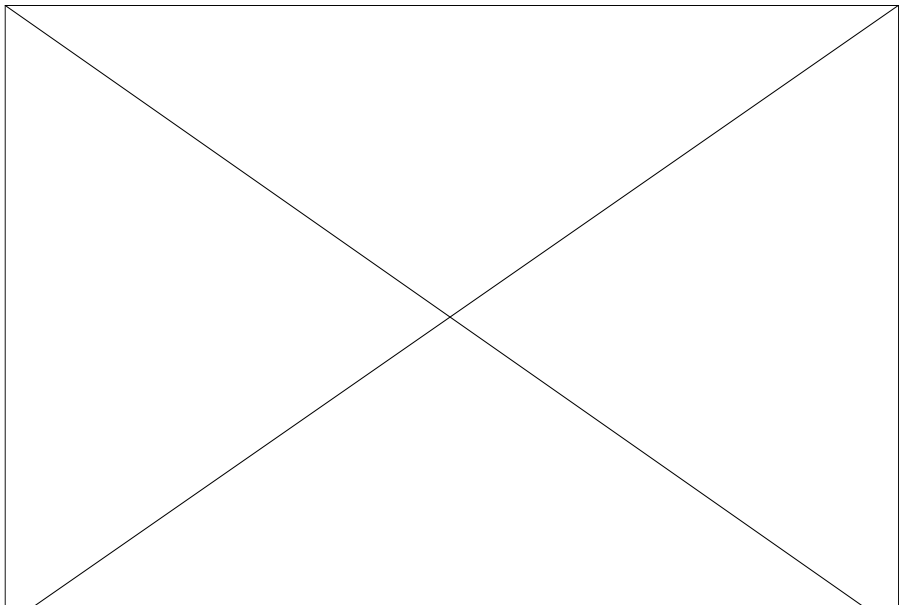

***Figure 3.6: Loading Assembly***

At each end where the load was applied, a K-brace cross frame with double 3 in. x 2 in. x 1/4 in. angles was attached as shown in Figure 3.8. This k-brace was designed to carry most of the load from the bottom flange of the girder to the tops of the webs, eliminating the potential for web crippling near these concentrated load points. In addition, the K-brace prevented lateral movement of the top flanges at the ends. The angles were attached to a 6 in. x 3/8 in. plate at the top and a WT 7 x 26.5 at the bottom, which was welded to the bottom flange of the girder. The WT-section also helped prevent local bending of the bottom flange where the roller applied the load.

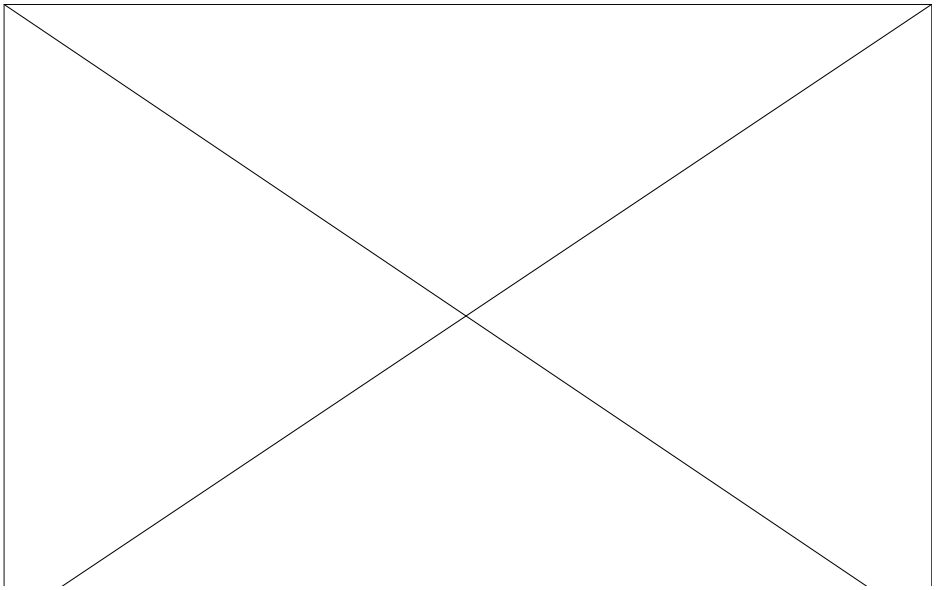

***Figure 3.7: Cross-Frame at Support Location***

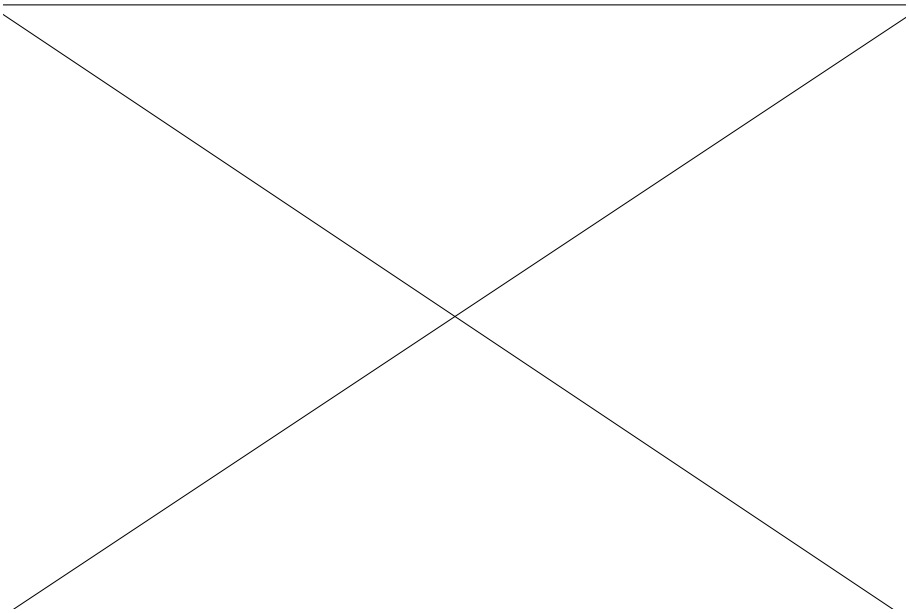

***Figure 3.8: K-brace at Load Point***

Two exterior frames or “stops” were constructed to limit lateral deflection of the top flanges during testing. Each stop was a truss consisting of 3 in. x 2 in. x 1/4 in. angles which were bolted to the laboratory floor, as shown in Figure 3.9. The stops were set to limit top flange deflection, and were adjusted during each test so that they did not come into contact with the top flanges. One stop frame was located at the south quarter-point of the center span, and the other stop frame was located near the centerline of the center span.

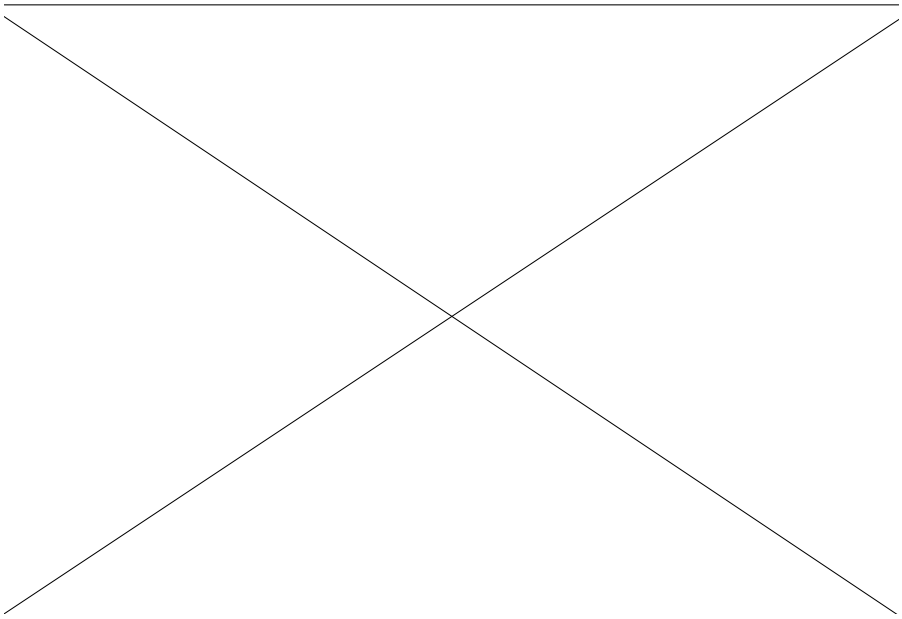

***Figure 3.9: Lateral Deflection Stops***

### 3.4 INSTRUMENTATION

During testing, lateral deflections, vertical deflections, strains, and load were monitored electronically using a computerized data acquisition system. In addition, lateral deflection on the west flange of the girder was monitored using a transit and load was monitored with a hydraulic pressure gage.

The lateral deflection of each top flange was measured at the quarter points of the interior span using electronic linear displacement string potentiometers. These lateral displacement gages were placed on rigid fixtures at the height of the top flanges and were connected to the top flanges using piano wire, as shown in Figure 3.10. They were located more than three feet away from the girder in order to minimize the effect of the vertical displacement of the girder on the lateral deflection readings. However, the vertical component of the gage

displacement was accounted for when the data was reduced using the vertical deflection readings taken at the corresponding gage locations. The gages had an accuracy of 0.001 inches. The gages were numbered and located as shown in Figure 3.11.

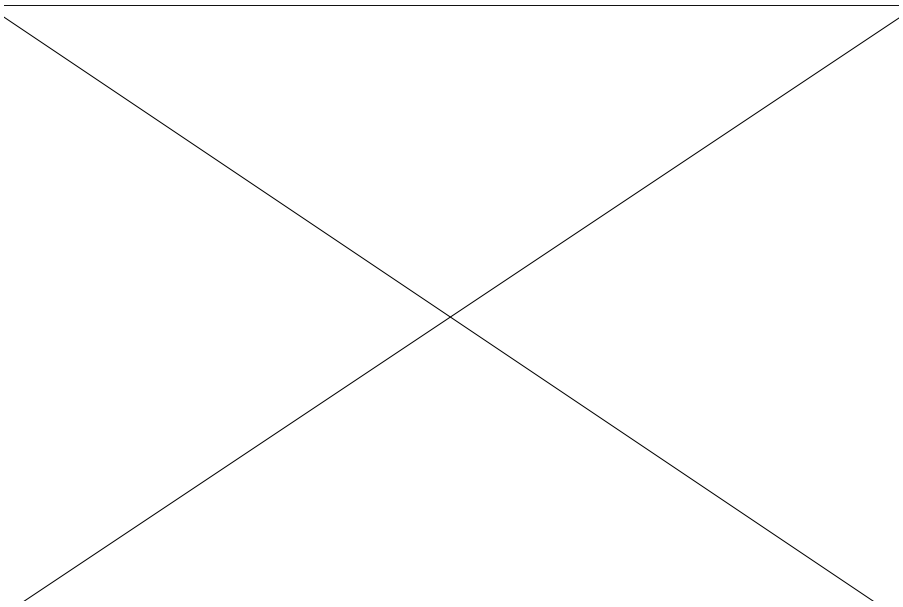

***Figure 3.10: Lateral Displacement Gages Attached to Rigid Frame***

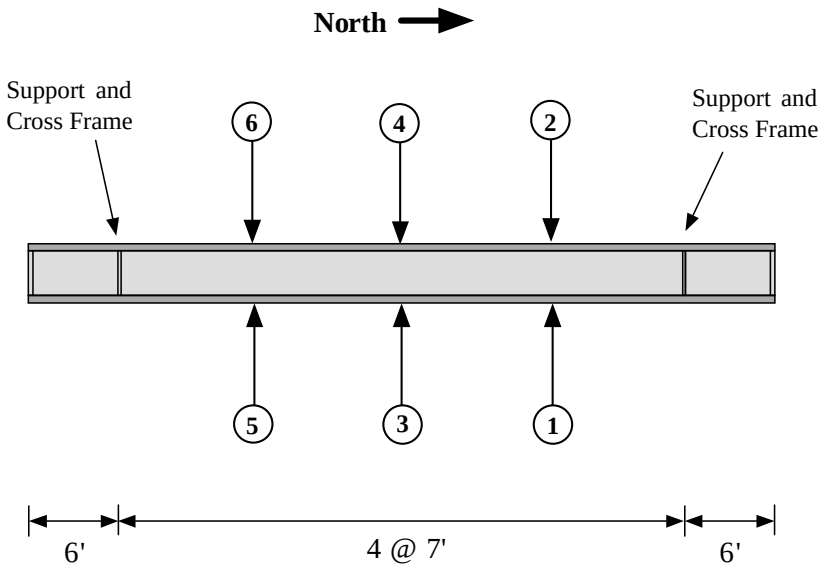


***Figure 3.11: Plan View of Girder Showing Location of Lateral Displacement Gages***

Lateral deflection of the west top flange was also measured using a transit. The transit was sighted parallel to the top west flange and lateral movements were measured using a scale placed against the flange. The transit readings were taken every 42 inches along the beam and could be read to an accuracy of 0.04 inches. The purpose of these measurements was to establish the buckled shape along the length of the girder.

Vertical deflections were measured using electronic linear displacement potentiometers, as shown in Figure 3.11. These gages were placed at the quarter points and the support locations as shown in Figure 3.12. A true measurement of deflections in the center span of the girder was calculated by adding the uplift at the supports to the interior span deflection readings. Rotation of the girder at the

supports could be calculated using readings from the gages placed on each side of the support. The vertical gages read deflection to an accuracy of 0.001 inches.

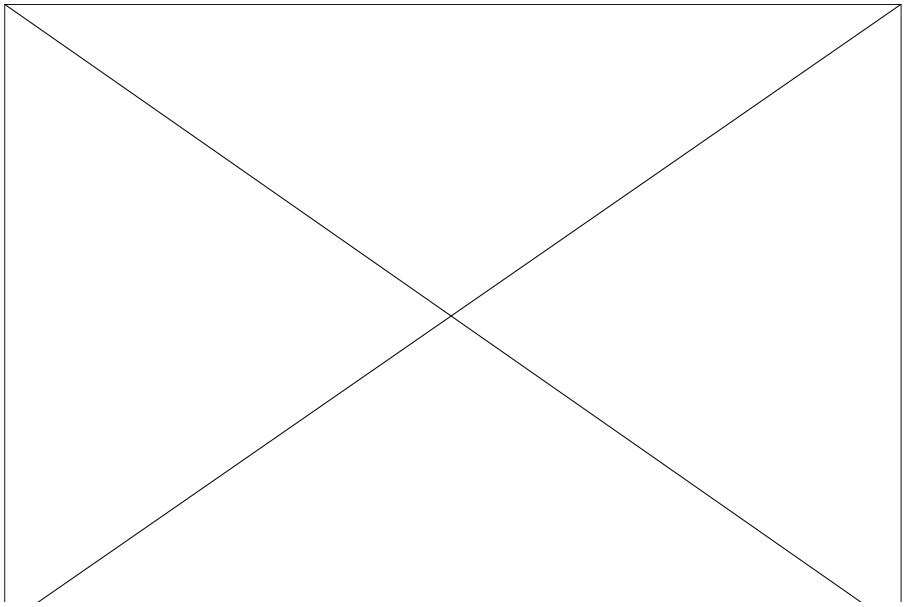

***Figure 3.11: Electronic Linear Potentiometer to Measure Vertical Deflection***

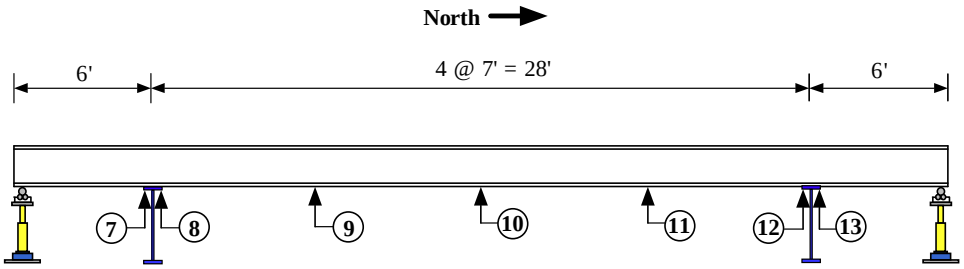


***Figure 3.12: Vertical Displacement Measurement Locations***

For tests involving the rectangular girder, strains were measured in the top flanges at the north quarter point using electronic resistance strain gages. Two gages were placed on the top of each flange near the edges and were monitored

during the test to identify when the yield load was approaching. Strain readings were not taken during tests of the trapezoidal girder.

Load was measured using a load cell placed between the ram and the floor. The load cell had a capacity of 200 kips and a precision of 100 pounds. A calibrated pressure gage measured the hydraulic pressure in the rams to provide a secondary measure of load.

### 3.5 BRACING

In addition to studying the buckling behavior of unbraced U-girders, several experiments were performed to determine the effects of increasing local web and bottom flange stiffness.

A set of exterior bolt-on braces was constructed to act as web and bottom flange stiffeners. Each brace consisted of three 2 in. x 2 in. x 1/8 in. angles which were bolted together to form a U-shaped frame. This frame was then bolted to the webs and bottom flange through holes in the girder using 1/2 in. diameter bolts. Four bolts were used to connect each web stiffener, and three bolts for the bottom flange stiffener. The bottom flange stiffener was bolted to the two web stiffeners with two bolts to prevent any change in the angle between the webs and the bottom flange. The bolts were hand-tightened. For a 1/2 in. diameter bolt, the minimum bolt tension necessary for a slip-critical connection can usually be achieved by hand tightening. The angles had a moment of inertia $I_x = 0.19$ in$^4$. A typical brace is shown in Figure 3.13.

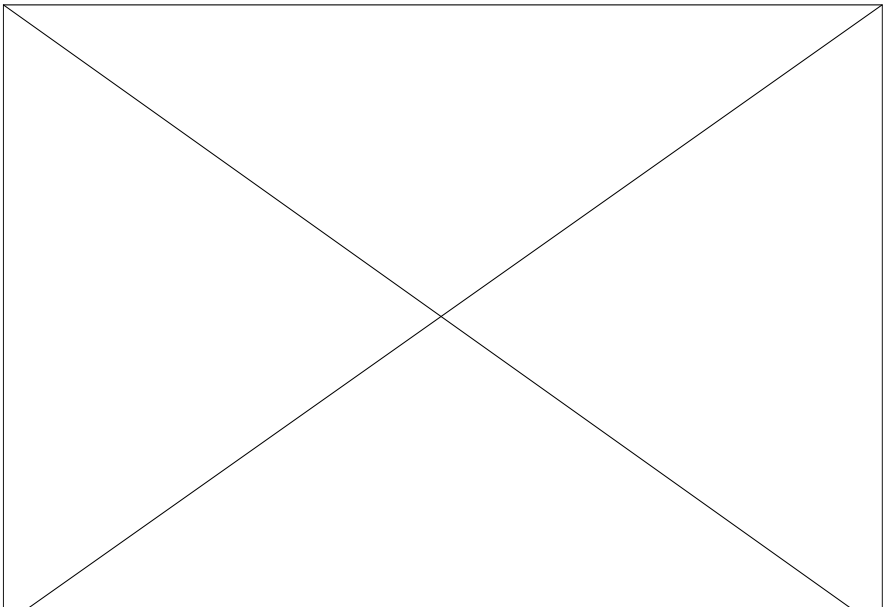

***Figure 3.13: Bolt-on Braces.***

Two bracing configurations were tested. The first consisted of braces placed at the first and third quarter-points of the center span. The second configuration involved three sets of braces placed at the first, second, and third quarter-points of the center span.

# CHAPTER 4

# Test Results

## 4.1 Determination of Buckling Load

The two test beams used for the experimental program were designed to buckle elastically, that is, buckle at loads less than the yield moment $M_y$ of the beam. This would allow numerous tests to be performed on a single test specimen without causing any permanent deformation. However, because the top flanges of the beam are not perfectly straight, some lateral deflection of the flanges occurs as load is applied. The lateral displacement causes additional P-Δ moments in the top flanges which add to the in-plane stresses and can lead to yielding before the buckling load has been reached. Therefore, the buckling load typically cannot be reached experimentally without some plastic deformation of the top flanges.

Southwell (1932) showed that it is possible to predict the buckling load of an initially imperfect column without testing it to failure. Based on the relationship between load and lateral deflection, Southwell developed a plotting technique which predicts the buckling load for initially-curved members. For example, the buckling load of a column could be determined to be 200 k even though a load of only 150 k was applied during an experiment.

### 4.1.1 Southwell Method

No lateral deflection occurs in a perfect column until the Euler load, $P_E$, is reached, as shown in Figure 4.1. For a column with a small initial imperfection, the column will have some lateral deflection as load is applied and will eventually carry the Euler load. For a column with a large initial imperfection, the P-Δ moments will cause yielding before the Euler load is reached.

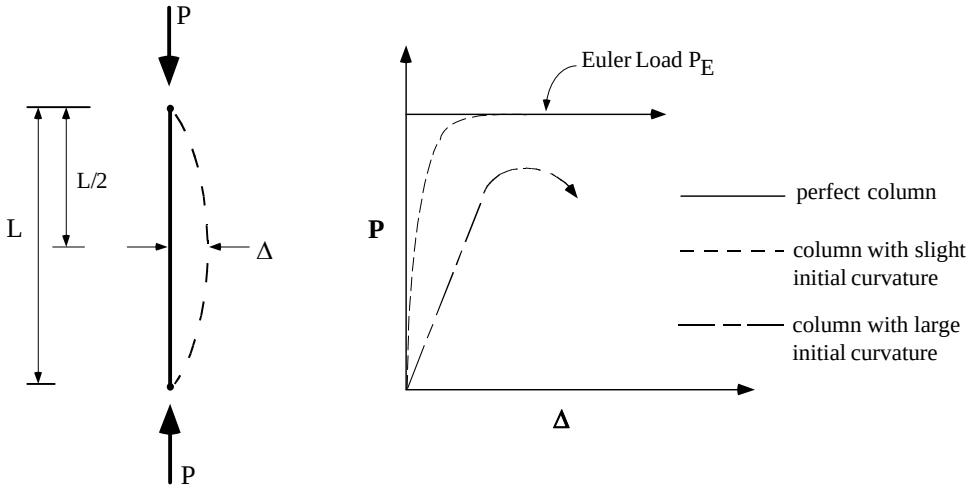


***Figure 4.1: Column Behavior***

Southwell represented the initial shape of the column as a half-sine wave with an initial midspan imperfection of $\Delta_0$. Based on this initial shape, the load-deflection relationship for a column can be approximated (Timoshenko, 1961) as:

$$\Delta = \frac{P}{P_E}\left[\frac{\Delta_0}{1-\frac{P}{P_E}}\right] \tag{4.1}$$

where Δ is the lateral deflection, $P_E$ is the Euler buckling load, and P is the axial load applied to the column. Equation 4.1 can be rearranged into the form:

$$\frac{\Delta}{P} P_E - \Delta = \Delta_0 \tag{4.2}$$

Considering Δ/P and Δ as variables, Equation (4.2) can be plotted as shown in Figure 4.2. This Southwell plot gives a straight line for load-deflection data points within the elastic range. The inverse of the slope of this line is the buckling load. This method can predict the buckling load to within about 2%, depending on how much load is applied during the experiment.

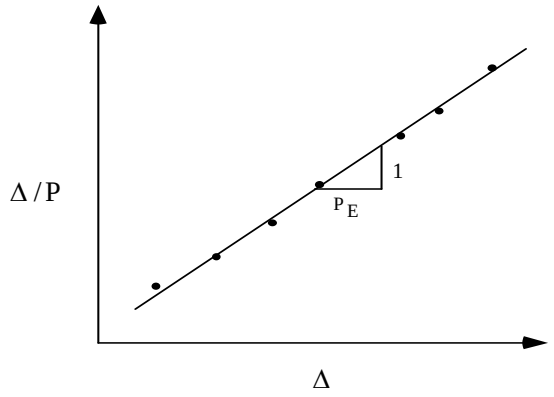


***Figure 4.2: Southwell Plot***

The Southwell plotting method is not limited to columns. The method can be used for any type of buckling problem with a hyperbolic load-deflection response that is similar to Equation (4.1). All that is needed is data relating load to deflection, rotation, or twist. Trahair(1969) and Meck(1977) successfully used the method or variations of it to predict buckling loads for beams.

For the U-girder tests in this experimental program, moment was used as a measure of load in Equation (4.1) since it is proportional to the in-plane stress in the top flange of the girder.

## 4.2 RECTANGULAR GIRDER TESTS

A series of three tests were performed on the rectangular U-girder described in Chapter 3. The tests examined unstiffened buckling behavior and the effects of stiffeners.

### 4.2.1 Initial Imperfections

The initial imperfections of the top flanges of the rectangular girder were measured using a transit with a line of sight parallel to the two supports. The imperfections for the east and west top flanges of the rectangular girder are shown in Figures 4.3 and 4.4, respectively. The maximum imperfection was 0.31 inches over the 28 ft center span, a ratio of 1/1083. This is within the out-of-straightness tolerances for compression members of 1/1000 given in the AISC Code of Standard Practice.

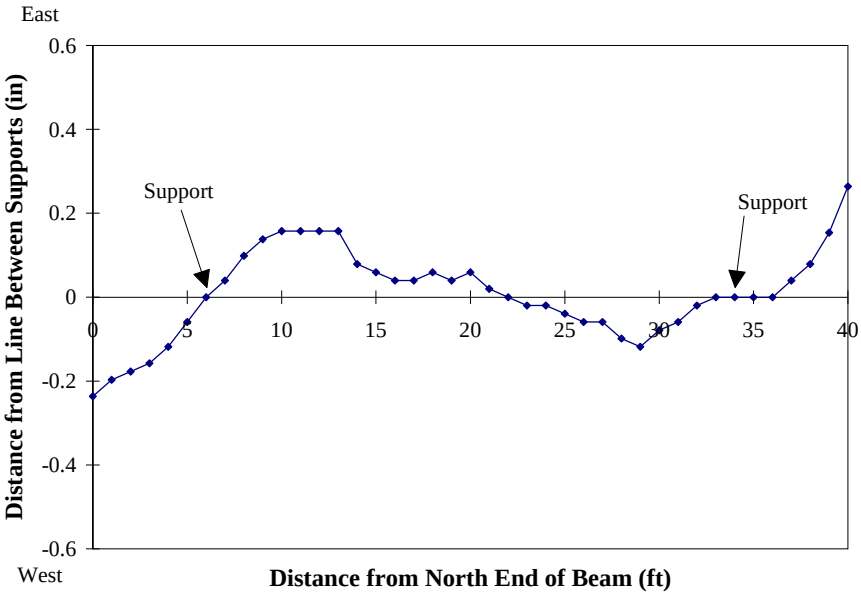


***Figure 4.3: Initial Imperfections of Rectangular Girder East Top Flange***

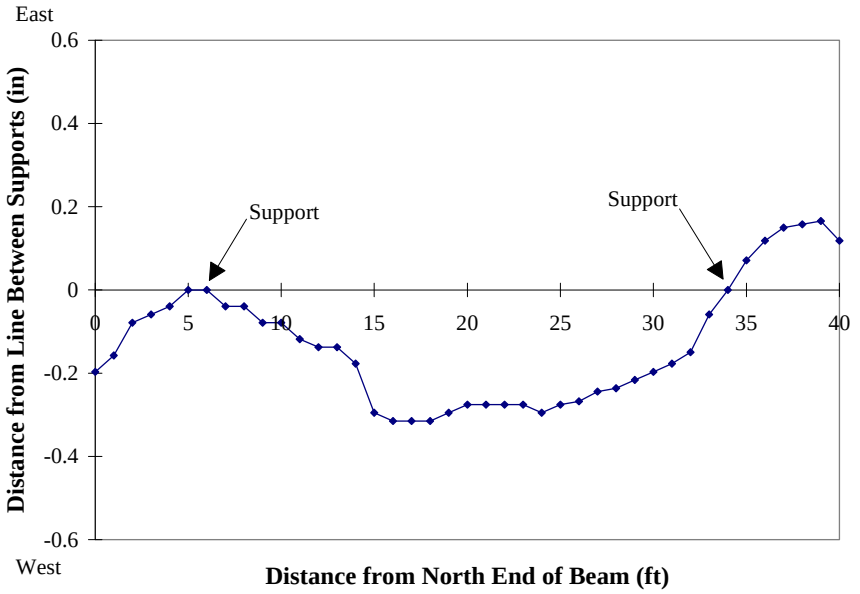


***Figure 4.4: Initial Imperfections of Rectangular Girder West Top Flange***

### 4.2.2 Test R1

Test R1 featured the unstiffened rectangular girder with a uniform moment applied as described in Chapter 3. The top flanges of the girder displaced laterally as load was applied. Load was increased until the strains measured in the top flanges of the girder were close to the yield strains of the steel. The maximum load applied to the girder was 3188 k-in which corresponds to an average top flange stress of 20 ksi.

The vertical deflection of the girder was measured and the centerline deflection is plotted versus average top flange stress in Figure 4.5. Stresses were determined using average strain gage readings and also were calculated from the load using bending theory. The stresses calculated for the loads were within 7% of the average stress given by the strain gages. The relatively straight lines of Figure 4.5 indicate that the girder behaved elastically throughout the test.

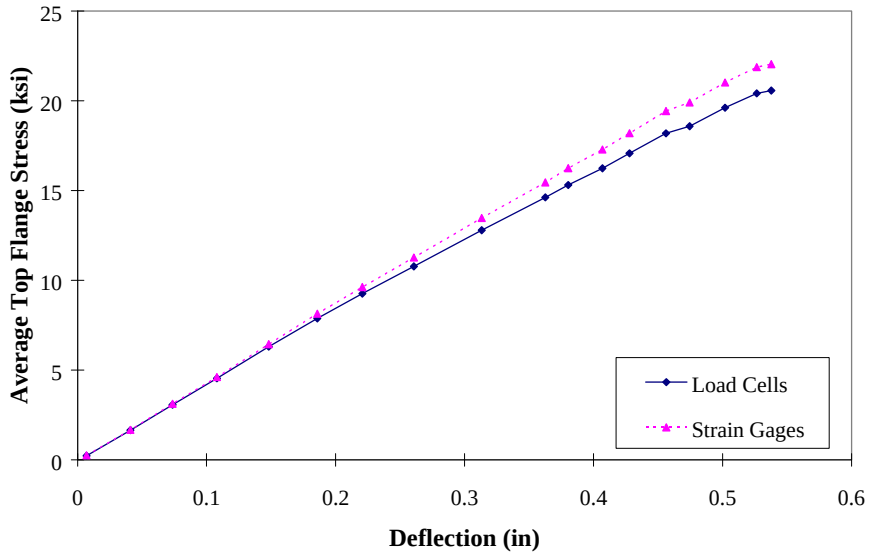


***Figure 4.5: Centerline Vertical Deflection For Test R1***

As the load was increased, each top flange deformed into a two-wave shape between the supports. The shape was visible with the naked eye near the maximum load stage. The top flanges were white-washed so that the deformed shapes would be more visible and any yielding could be detected. Figure 4.6 shows the deformed shape of the east top flange (looking south) near the maximum load stage. The deflected shape of the west top flange was measured at load stages using a transit. The west flange transit readings for the zero and maximum load stages are presented in Figure 4.7. For the west flange, the initial imperfection was a one-wave shape between the supports, as shown in Figure 4.4. As load was applied, the west flange began to change into a two-wave shape. The transit readings show that the top flange at the north end of the center span began to move to the east while the south end moved west. The node of the deformed shape moved towards the middle of the span as load was increased.

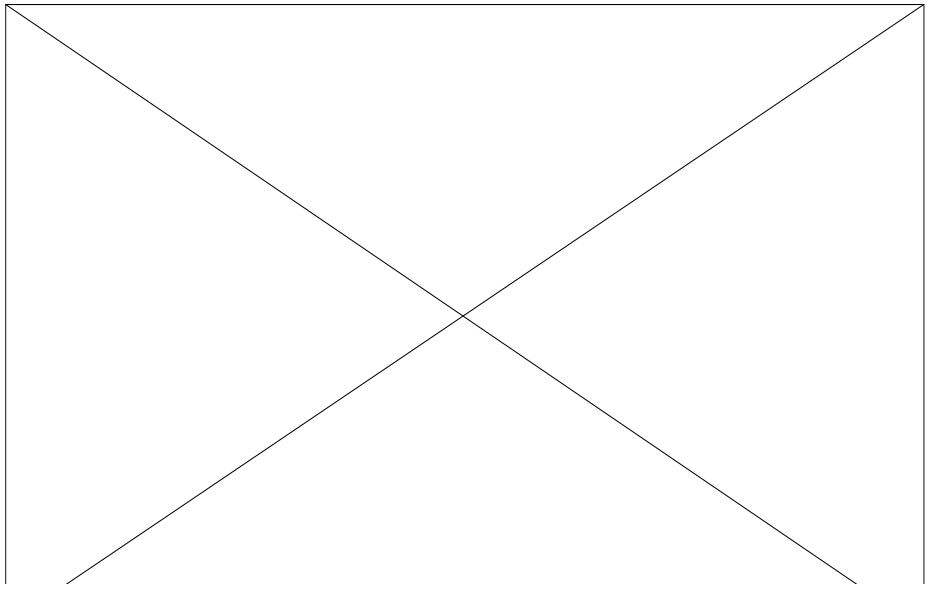

***Figure 4.6: East Flange Deformed Shape at Maximum Applied Load***

Lateral deflection measurements were also taken using potentiometers as described in Chapter 3. Load versus lateral deflection data for the north and south quarter-points are plotted in Figure 4.8. The plot shows that the top flanges were both displacing in the east direction at the north quarter-point and in the west direction at the south quarter-point. These readings also indicate that the flanges were deforming into a two-waved shape.

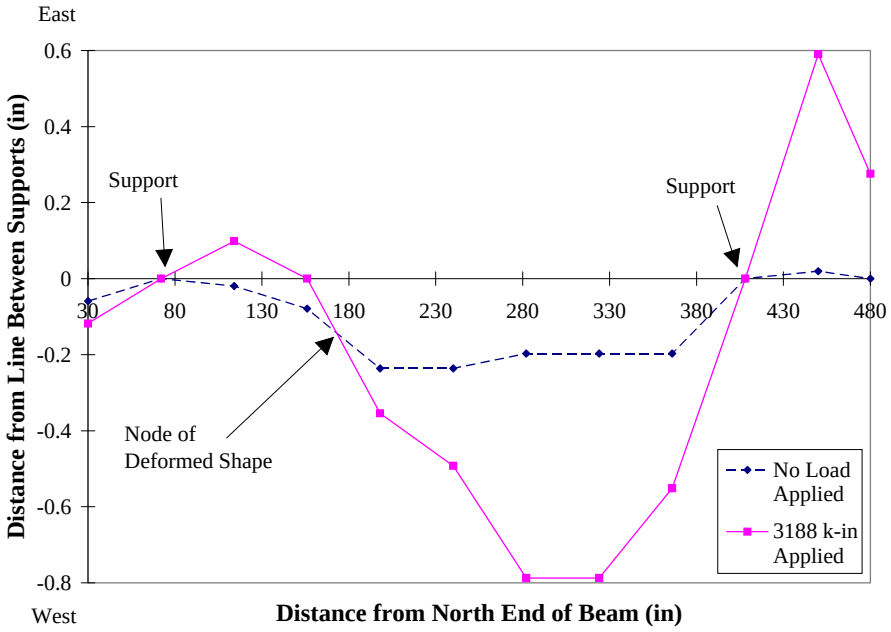


*Figure 4.7: West Flange Deformed Shape for Test R1*

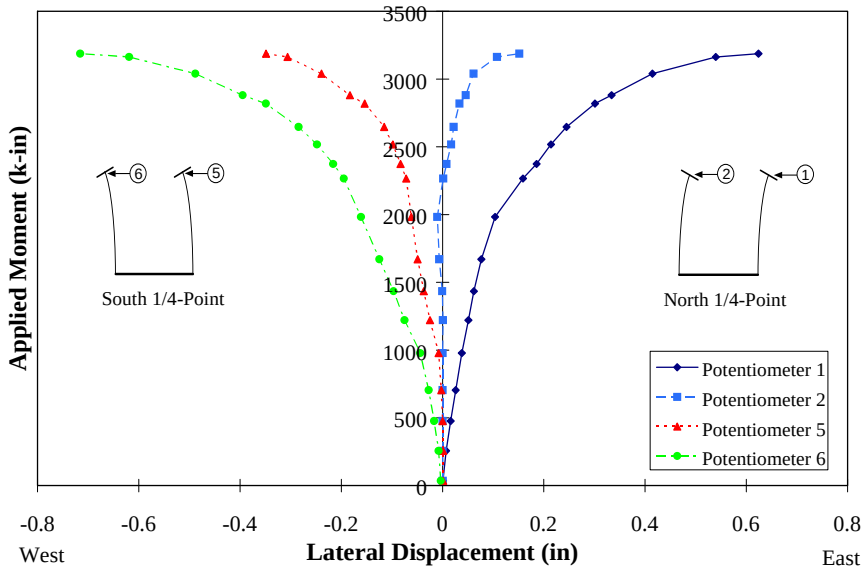


*Figure 4.8: Lateral Deflection of Top Flanges at North and South Quarter-Points for Test R1*

Southwell plots were created using the load-deflection data from the six potentiometers measuring lateral deflection. A Southwell plot for string pot 1 is provided in Figure 4.9. A linear regression analysis was used to fit a line through the data points. The inverse of this best-fit line's slope is the predicted buckling load.

At the beginning of each test, some uplift and settling of the test fixtures occurs. These data points do not align with the data points at latter stages of loading on the Southwell plot, and were not included in the regression analysis. The length of the best-fit line in Figure 4.9 indicates which data points were used for the regression analysis.

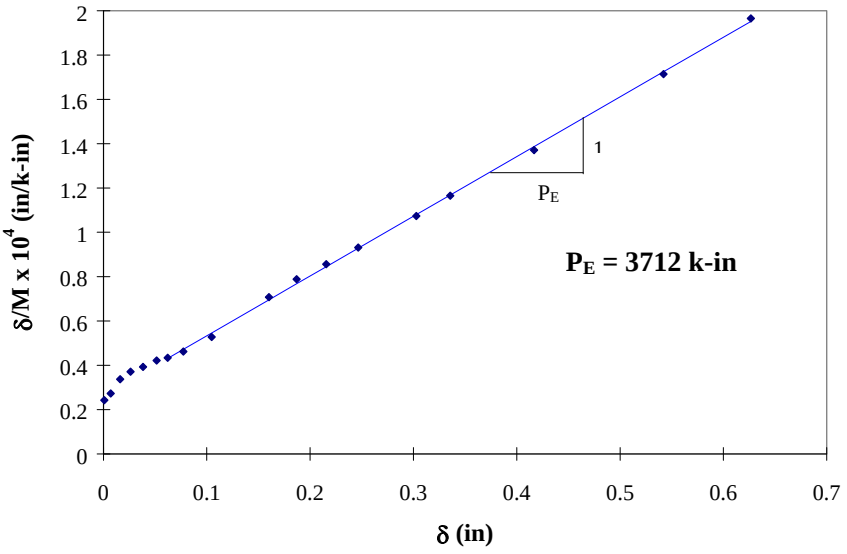


***Figure 4.9: Southwell Plot for Test R1, Potentiometer 1***

Potentiometer 2 measures lateral deflection at the north quarter-point of the girder span. As shown in Figure 4.7, the node of the deformed shape for the

west flange occurs near the location of this pot. At this location the top flange deflections are very small and sometimes switch direction as load is applied. The Southwell plot does not give good results for data near these node points. Therefore, data collected near a node of the deformed shape were not included in the calculation of the average buckling load. For the east flange, the initial imperfection was a two-wave shape with a node near the center of the girder. Thus data from string pot 3 was also not included in the calculation of the average for any of the rectangular girder tests.

Table 4.1 provides a summary of Southwell results for test R1. The average buckling load was determined to be 3703 k-in.

***Table 4.1: Southwell Results for Test R1***

| Potentiometer No. | Southwell Buckling Load (k-in) | Loads Used for Average (k-in) | Difference from Average |
|---|---|---|---|
| 1 | 3712 | 3712 | 0.2 % |
| 2 | 3323 | --- | --- |
| 3 | 3720 | --- | --- |
| 4 | 3746 | 3746 | 1.2 % |
| 5 | 3625 | 3625 | 2.1 % |
| 6 | 3730 | 3730 | 0.7 % |
| Average Buckling Load = | | 3703 | --- |

### 4.2.3 Tests R2 and R3

Tests R2 and R3 featured the rectangular girder with 2 in. x 2 in. x 1/8 in. braces as described in Chapter 3. Braces were attached at the north and south

quarter-points for test R2, and a third brace was added at the center of the span for test R3.

For both tests, the top flanges of the girder deformed into a two-wave shape similar to the shape during test R1. Plots of the top flange lateral deflection and the west flange displaced shape for tests R2 and R3 can be found in Appendix A.

The Southwell results for test R2 are presented in Table 4.2. The average buckling load for this test was 4246 k-in, 14.6% higher than the unstiffened case. The maximum load applied to the test specimen was 3516 k-in, which is 83% of the average Southwell buckling load.

***Table 4.2: Southwell Results for Test R2***

| Potentiometer No. | Southwell Buckling Load (k-in) | Loads Used for Average (k-in) | Difference from Average |
|---|---|---|---|
| 1 | 4084 | 4084 | 3.8 % |
| 2 | 4082 | --- | --- |
| 3 | 3584 | --- | --- |
| 4 | 4529 | 4529 | 6.7 % |
| 5 | 4197 | 4197 | 1.2% |
| 6 | 4175 | 4175 | 1.7% |
| Average Southwell Buckling Load = | | 4246 | --- |

Table 4.3 gives the Southwell results from test R3. The average buckling load was 4486 k-in, 21.1% higher than the unstiffened case. The maximum load applied to the girder was 3500 k-in.

***Table 4.3: Southwell Results for Test R3***

| Potentiometer No. | Southwell Buckling Load (k-in) | Loads Used for Average (k-in) | Difference from Average |
|---|---|---|---|
| 1 | 4086 | 4086 | 8.9 % |
| 2 | 3939 | --- | --- |
| 3 | 3823 | --- | --- |
| 4 | 4644 | 4644 | 3.5 % |
| 5 | 5020 | 5020 | 11.9 % |
| 6 | 4193 | 4193 | 6.5 % |
| Average Southwell Buckling Load = | | 4486 k-in | --- |

The Southwell results from tests R2 and R3 are less consistent than the results for test R1, the unstiffened girder. This may be due to changes in the load-displacement relationship caused by the braces attached at discrete locations. The Southwell method assumes that the displaced shape is related to a sine curve. The braces may affect this shape and lead to less consistent Southwell results.

## 4.3 TRAPEZOIDAL GIRDER TESTS

Two tests similar to tests R1 and R2 described above were also performed on the trapezoidal U-girder described in Chapter 3.

### 4.3.1 Initial Imperfections

The initial imperfections of the east and west top flanges of the trapezoidal girder are presented in Figures 4.10 and 4.11, respectively. The west flange of the

girder had an imperfection of 0.53 inches over the 28 ft center span, a ratio of about 1/600. This is greater than the 1/1000 limit for compression members.

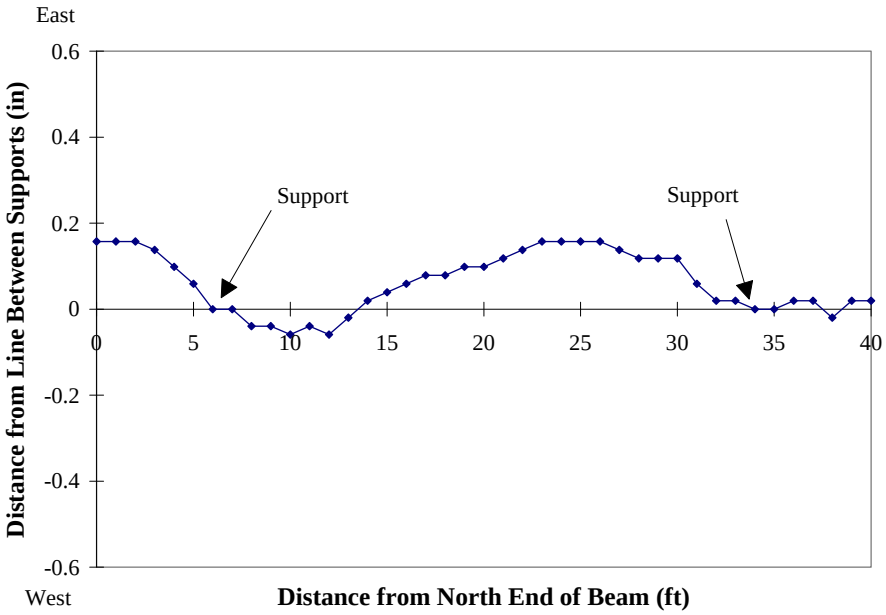


***Figure 4.10: Initial Imperfections of Trapezoidal Girder East Top Flange***

### 4.3.2 Test T1

Test T1 featured the unstiffened trapezoidal girder with a uniform moment applied as described in Chapter 3. The top flanges of the girder displaced laterally as shown in Figure 4.12. Unlike the rectangular girder, the top flanges of the trapezoidal girder deformed into a one-wave shape, with all points along the span moving to the west. Figure 4.13 shows that the initial imperfection of the west flange continued to grow in magnitude as load was applied, with no signs of changing into a two-waved shape. The maximum load applied to the girder was 2547 k-in.

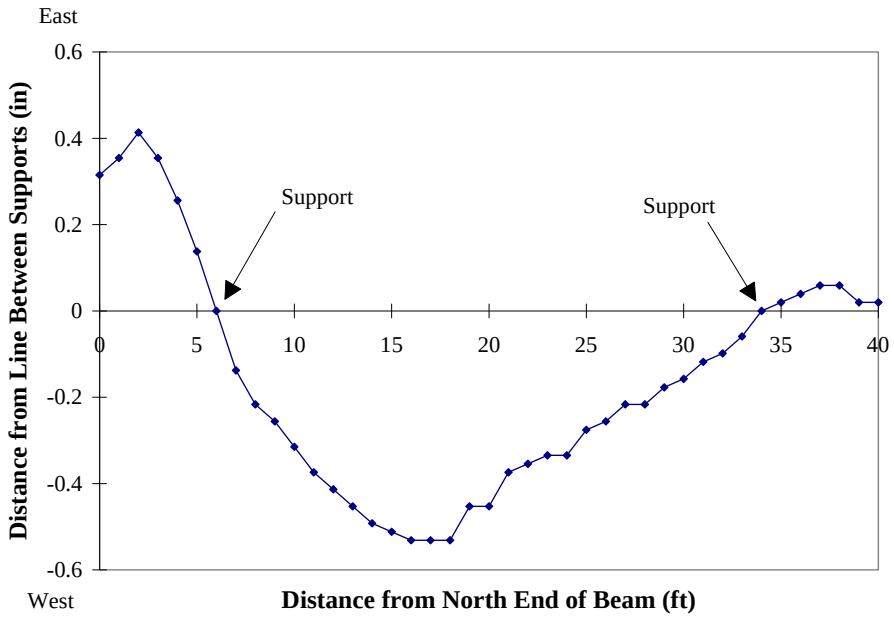


***Figure 4.11: Initial Imperfections of Trapezoidal Girder West Top Flange***

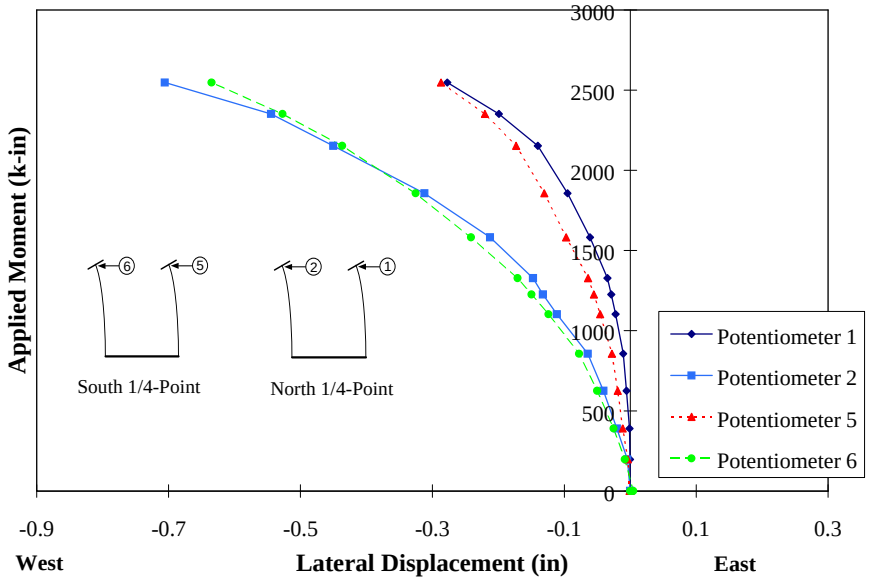


***Figure 4.12: Lateral Deflection of Top Flanges at North and South Quarter-Points for Test T1***

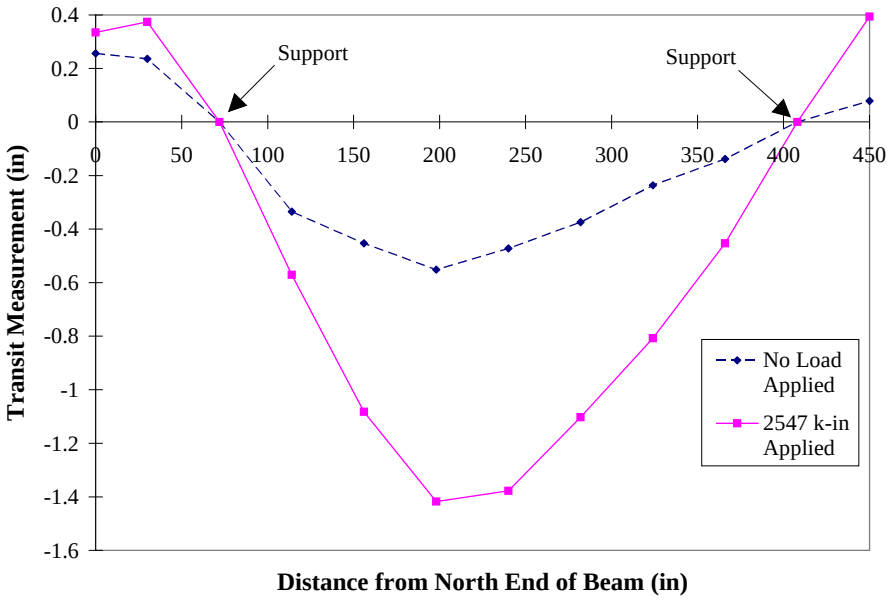


***Figure 4.13: West Flange Deformed Shape for Test T1***

Table 4.4 shows the Southwell results for test T1. Since there were no nodes occurring in the deformed shape, all string pots were included in the calculation of the average buckling load. The results are much less consistent than the results for test R1 of the rectangular girder.

Test T2 featured the trapezoidal girder with 2 in. x 2 in. x 1/8 in. braces attached at the north and south quarter-points, as in test R2. The Southwell results for test T2 are presented in Table 4.5. The average buckling load for this test was 4620 k-in, 35.7 % higher than the unstiffened case. However, the results are very scattered. The Southwell plots give values ranging from 14% to 56% above the unstiffened test T1.

***Table 4.4: Southwell Results for Test T1***

| String Pot No. | Southwell Buckling Load (k-in) | Loads Used for Average (k-in) | Difference from Average |
|---|---|---|---|
| 1 | 2982 | 2982 | 12.4 % |
| 2 | 3393 | 3393 | 0.3 % |
| 3 | 3034 | 3034 | 10.8 % |
| 4 | 3528 | 3528 | 3.7 % |
| 5 | 3570 | 3570 | 4.9 % |
| 6 | 3909 | 3909 | 14.9 % |
| Average Buckling Load = | | 3403 | --- |

***Table 4.5: Southwell Results for Test T2***

| String Pot No. | Southwell Buckling Load (k-in) | Loads Used for Average (k-in) | Difference from Average |
|---|---|---|---|
| 1 | 3867 | 3867 | 16.3 % |
| 2 | 4707 | 4707 | 1.9 % |
| 3 | 3987 | 3987 | 13.7 % |
| 4 | 4707 | 4707 | 1.9 % |
| 5 | 5318 | 5318 | 15.1 % |
| 6 | 5132 | 5132 | 11.1 % |
| Average Buckling Load = | | 4620 | --- |

# CHAPTER 5

# Analysis of Test Results

## 5.1 Comparison of Test Results with Eigenvalue Analyses

The dimensions of the finite element models presented in Chapter 2 were adjusted to the measured dimensions of the test specimens. The average measured cross-section dimensions of the rectangular and trapezoidal U-girders presented in Chapter 3 were used in the ABAQUS finite element models. The bolt-on angle stiffeners used in the experimental program were modeled as rectangular plates in the finite element model. These stiffener plates had the same bending stiffness as the bolt-on angles.

Table 5.1 compares the experimental results for the rectangular U-girder to ABAQUS eigenvalue buckling loads. Table 5.2 compares the trapezoidal U-girder experimental results to the corresponding eigenvalue loads.

***Table 5.1: Comparison of Eigenvalue Finite Element Analyses and Experimental Results for Rectangular Girder***

| Test No. | Max. Load Applied During Test (k-in) | Avg. Southwell Buckling Load (k-in) | ABAQUS Eigenvalue Load (k-in) | Difference Between Southwell and Eigenvalue |
|---|---|---|---|---|
| R1 | 3188 | 3703 | 2705 | 37 % |
| R2 | 3516 | 4246 | 2936 | 45 % |
| R3 | 3500 | 4486 | 3704 | 21 % |

***Table 5.2: Comparison of Eigenvalue Finite Element Analyses and Experimental Results for Trapezoidal Girder***

| Test No. | Max. Load Applied During Test (k-in) | Avg. Southwell Buckling Load (k-in) | ABAQUS Eigenvalue Load (k-in) | Difference Between Southwell and Eigenvalue |
|---|---|---|---|---|
| T1 | 2547 | 3403 | 2562 | 33 % |
| T2 | 2788 | 4620 | 2672 | 73 % |

The tests of both U-shaped girders gave Southwell buckling loads which were significantly greater than the eigenvalue loads predicted by the finite element models. The Southwell buckling loads from the laboratory tests exceeded the eigenvalue loads by as much as 73%. However, the Southwell method will not give accurate results for cases where the deformed shape is not some form of a sine curve. The U-girder's initial imperfections and attached stiffeners may lead to changes in the deformed shape and error from the Southwell method. The accuracy of the Southwell method is discussed further in Section 5.3.

Regardless of the Southwell predictions for the buckling load, the loads applied to the U-girders for several of the tests exceeded the eigenvalue buckling loads. For tests R1 and R2, the loads applied during the experiments were 20% greater than the eigenvalue loads. In an attempt to understand these differences, a series of large displacement finite element analyses were performed.

## 5.2 COMPARISON OF TEST RESULTS WITH LARGE DISPLACEMENT ANALYSES

The results presented above give eigenvalue buckling loads for finite element models of the U-shaped test specimens. The eigenvalue buckling load for a beam is analogous to the Euler buckling load for a column; that is, it is the load at which a perfectly straight member becomes unstable and failure occurs. The eigenvalue analysis does not provide any load-displacement history for a member or recognize the effects of initial imperfections. To examine the load-displacement behavior of a member, a "large displacement" finite element analysis can be used.

A large displacement analysis consists of loads applied to the model in discrete increments or time steps. For each time step, the load is increased slightly and a corresponding displacement is calculated based on the stiffness of the model. The ABAQUS analysis uses large displacement theory which can account for significant changes in the geometry of the member as the load is increased. A complete load-displacement history for a model, including post-buckling behavior, can be generated with this type of analysis. The effects of initial imperfections can also be studied by including these imperfections in the model geometry.

### 5.2.1 Large Displacement Analysis of Rectangular U-shaped Girder

A large displacement analysis was performed to investigate the effects of the U-girder's top flange out-of-straightness. The top flanges of the rectangular girder model were modified to include the rectangular test specimen's initial imperfections shown in Figures 4.3 and 4.4. An elastic large displacement

analysis was performed using this modified geometry. Figure 5.1 shows the lateral displacement of the top flange at the southwest quarter-point (which corresponds to the location of pot 6) plotted versus load for the finite element model (FEM) of the rectangular girder.

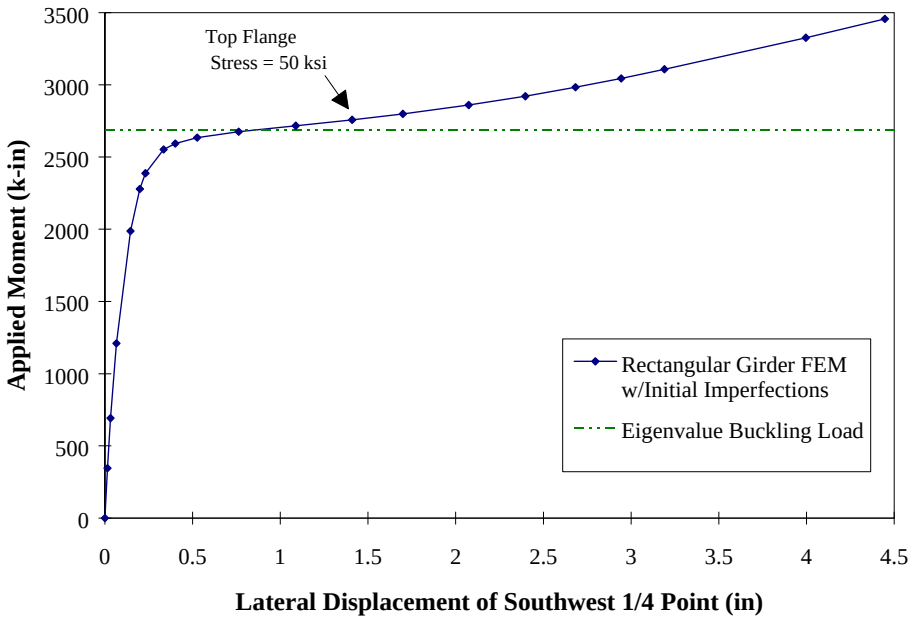


***Figure 5.1: Load vs. Lateral Displacement of Southwest Quarter-Point for Rectangular Girder Large Displacement Analysis***

Initially, very little lateral movement occurred as load was applied to the model. As the applied load approached the eigenvalue buckling load, a dramatic decrease in the slope of the load versus lateral displacement curve occurred. The slope then began to increase as larger lateral displacements were reached. Figure 5.1 indicates that this rectangular U-girder model has a significant post-buckling capacity at larger lateral displacements. At a lateral displacement of 3.5 inches, the load applied to the girder was 15% greater than the eigenvalue buckling load.

However, out-of-plane bending in the top flanges causes stresses which exceed the yield stress for the material before this post-buckling strength can be realized. Yielding would occur in the top flanges at loads just 2% larger than the eigenvalue load for this girder, as shown in Figure 5.1. The effects of yielding are not included in this elastic analysis, so the large displacement results would be invalid beyond displacements of 1.4 in.

The two-wave buckled shape of the top flanges is illustrated in Figure 5.2. At a given cross-section, the top flanges both displaced in the same direction. This is the same type of deformed shape which occurred during laboratory test R1. This shape corresponds with the second eigenvalue buckling mode for the rectangular girder presented in Chapter 2. In the first mode the girder deformed into a two-wave shape with the top flanges displacing in opposite directions at any given cross-section. As noted in Chapter 2, there is only a 0.5% difference in load between the first and second modes. The girder's initial imperfections caused the second buckling mode to occur in the large displacement analysis just as in the laboratory test.

A comparison of the rectangular girder large displacement analysis and laboratory test R1 is shown in Figure 5.3. The behavior of the finite element model corresponds closely with the test R1 results for loads less than 2400 k-in. As the applied load nears the eigenvalue buckling load of 2705 k-in, the slope of the load-displacement curve for the finite element model decreases significantly, while the test R1 curve changes gradually. The test specimen reached a load of 3188 k-in at a lateral displacement of 0.71 inches. The load applied during the

laboratory test was 20% greater than the load of the finite element model for the same displacement.

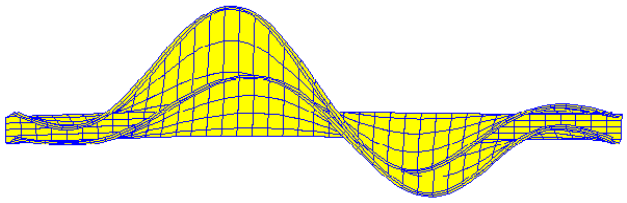

***Figure 5.2: Buckled Shape of Rectangular Girder Model for Large Displacement Analysis***

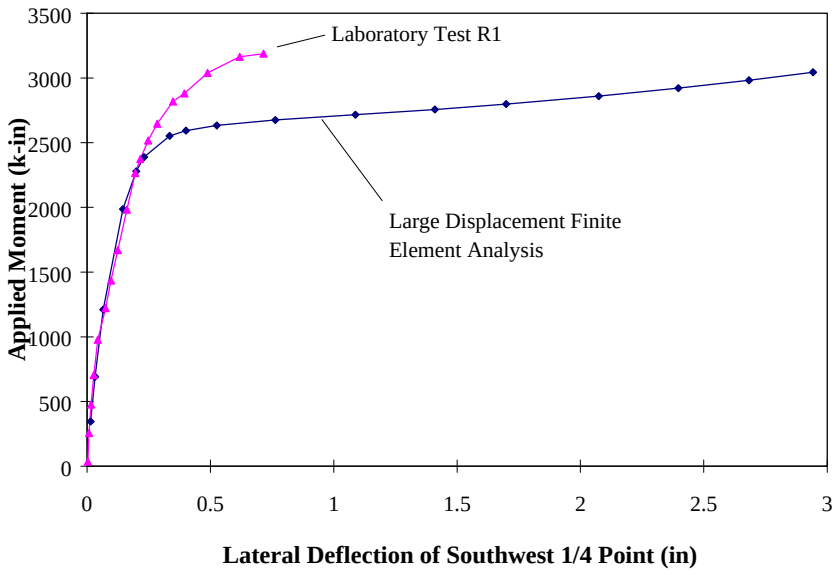


***Figure 5.3: Comparison of Large Displacement Analysis and Test R1***

### 5.2.2 Effects of Top Flange Initial Imperfections

Several other top flange imperfections were input into the finite element model to study the U-girder's sensitivity to various imperfection shapes and sizes.

Each of the models were based on the rectangular girder geometry, with only the shape of the top flanges modified. For clarity, the imperfections of the rectangular girder shown in Figures 4.3 and 4.4 will be called imperfection A in the following discussion. The imperfections of the trapezoidal girder, shown in Figures 4.9 and 4.10, will be called imperfection B.

The first analysis included imperfection A with the magnitude of the imperfections increased by 25%. A second analysis was performed using imperfection B. Finally, an analysis was carried out using just 20% of imperfection B. The results of these analyses are shown in Figure 5.3.

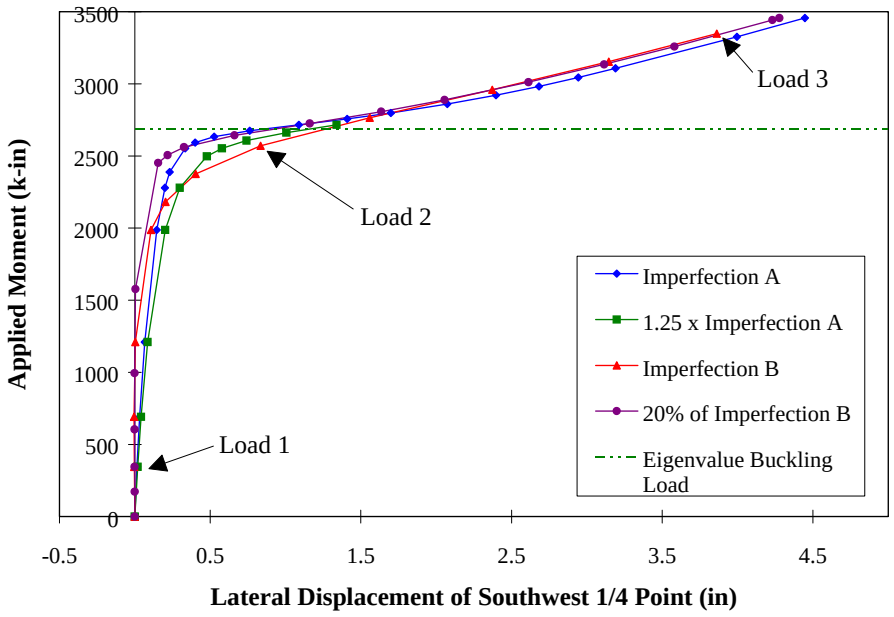


***Figure 5.4: Effects of Various Top Flange Imperfections on Rectangular Finite Element Model***

In general, all of the models behaved in a similar manner, regardless of their initial imperfections. The slope of the load-displacement curve varied slightly depending on the magnitude of the imperfection. Increasing imperfection A by 25% resulted in a decrease in the initial slope of the curve. Decreasing imperfection B by 80% resulted in a much steeper curve. However, after 1.5 inches of lateral displacement had occurred, the curves all followed a similar path.

The shape of the initial imperfection had little effect on the buckling load or buckled shape for the large displacement analysis. The initial shape of the west top flange for imperfections A and B was essentially a one-wave shape between the supports. As load was applied to the finite element model, this shape shifted from one-wave into two-waves. Figure 5.5 shows a normalized plot of the deformed shape for the west top flange at several load stages during the analysis. The load stages are illustrated on the load-deflection plot of Figure 5.4.

These large displacement analyses indicate that moderate imperfections of the top flanges do not have a significant impact on the buckling load for this U-shaped girder. Regardless of the initial shape or size of the imperfection, the large displacement analyses indicate a buckling load near 2700 k-in and a two-wave buckled top flange shape.

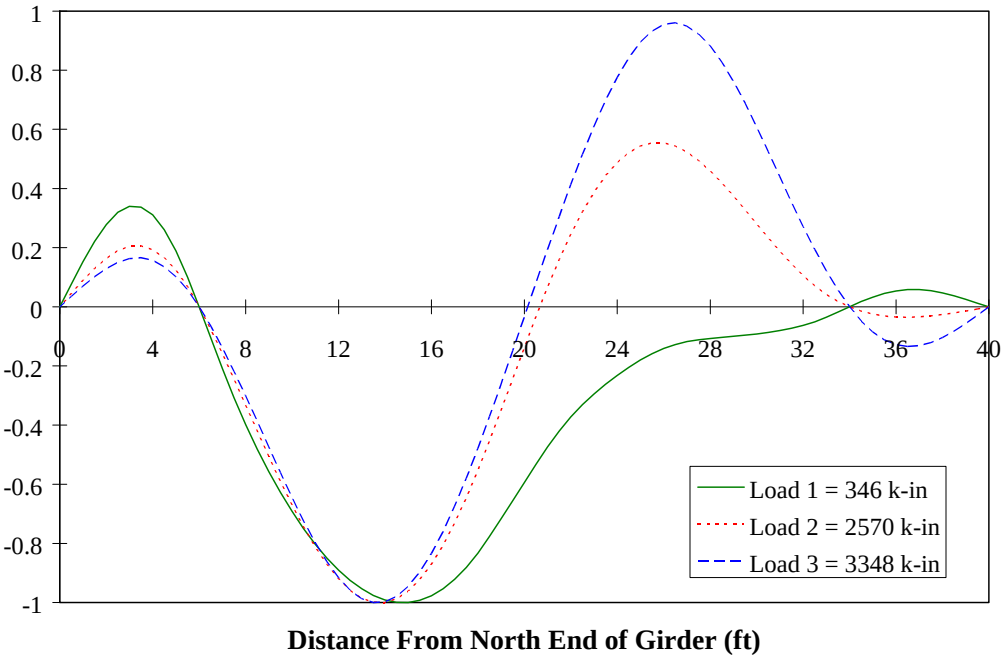


***Figure 5.5: Normalized Deflected Shape of West Top Flange for ABAQUS Model with Imperfection B***

## 5.3 EVALUATION OF SOUTHWELL PLOTS

A comparison of eigenvalue analyses and average Southwell results was presented in Tables 5.1 and 5.2. The Southwell results indicated buckling loads as much as 73% greater than eigenvalue buckling load. The results from the individual string pots presented in Chapter 4 were very inconsistent for most of the tests. It was noted that the Southwell method is accurate for cases where the deformed shape approximates a sine curve. However, because of initial

imperfections and stiffeners located at discrete cross-sections, the deformed shapes of the laboratory test specimens were not perfect sine curves.

Three large displacement analyses were performed to study the accuracy of the Southwell method for U-girder buckling tests. The analyses were simulations of the rectangular girder tests R1, R2, and R3, including top flange initial imperfections and stiffeners. Lateral displacement data was taken for the top flange nodes located at the quarter-points of the center span. These data correspond with the string pot data collected during the laboratory tests. A Southwell buckling load was determined from the theoretical load-displacement results, just as for the laboratory tests. The results for the simulation of tests R1, R2, and R3 are presented in Tables 5.3, 5.4, and 5.5 respectively.

***Table 5.3: Southwell Results for Large Displacement Simulation of Test R1***

| String Pot No. | Southwell Buckling Load (k-in) | Percent Difference from Average |
|---|---|---|
| 1 | 2807 | + 0.7 % |
| 2 | 2788 | + 0.1 % |
| 3 | 2741 | - 1.6 % |
| 4 | 2755 | - 1.1 % |
| 5 | 2858 | + 2.6 % |
| 6 | 2766 | - 0.7 % |
| Average Buckling Load = | 2786 | --- |
| Eigenvalue Buckling Load = | 2705 | - 2.9 % |

***Table 5.4: Southwell Results for Large Displacement Simulation of Test R2***

| String Pot No. | Southwell Buckling Load (k-in) | Percent Difference from Average |
|---|---|---|
| 1 | 2879 | + 1.6 % |
| 2 | 2848 | + 0.5 % |
| 3 | 2810 | - 0.7 % |
| 4 | 2803 | - 1.0 % |
| 5 | 2813 | - 0.7 % |
| 6 | 2843 | + 0.4 % |
| Average Buckling Load = | 2832.6 | --- |
| Eigenvalue Buckling Load = | 2935 | + 3.6 % |

***Table 5.5: Southwell Results for Large Displacement Simulation of Test R3***

| String Pot No. | Southwell Buckling Load (k-in) | Percent Difference from Average |
|---|---|---|
| 1 | 9218 | + 49.9 % |
| 2 | 4499 | - 26.8 % |
| 3 | 4279 | - 30.4 % |
| 4 | 8163 | + 32.8 % |
| 5 | 7583 | + 23.3 % |
| 6 | 3149 | - 48.8 % |
| Average Buckling Load = | 6148 | --- |
| Eigenvalue Buckling Load = | 3704 | - 39.8 % |

The Southwell results for simulations of tests R1 and R2 give consistent results for each pot location, with an average close to the eigenvalue for each case. This indicates that the Southwell buckling estimate from each pot would be an accurate indication fo the buckling load. The simulated Southwell results for R1 and R2 were within 2.9% and 4.1% of the respective eigenvalue solutions. The results from the test R3 analysis, however, are scattered. The average Southwell result is almost 40% greater than the eigenvalue solution. Only the pot 6 location gave a Southwell solution below the eigenvalue. All other locaations gave higher results. This analysis suggests that for some cases the attached braces (and perhaps the top flange imperfections) may cause deformed shapes which are

more complicated than the shape of a sine curve. The Southwell method is not useful in these cases.

## 5.4 Differences Between Finite Element Models and Test Setup

The data presented in section 5.1 showed there were significant differences between the eigenvalue buckling loads and the experimental test results. The loads applied during the laboratory tests exceeded the eigenvalue loads by as much as 20%. The large displacement finite element analyses presented in section 5.2 indicated that the imperfections of the top flanges do not lead to buckling loads higher than the eigenvalue, although the models did exhibit some post-buckling strength at higher lateral displacements. Thus, there seems to be some other source for the disparity between the finite element models and the laboratory tests.

The finite element models presented in this paper are simplifications of the actual laboratory specimens. The exact dimensions and imperfections at every point along each test specimen were not modeled. The boundary conditions for the models were approximated based on the laboratory test setup. In order to explain the experimental results, several of the differences between the finite element model and the laboratory tests were isolated and studied.

### 5.4.1 Warping Restraint

The boundary conditions of the finite element model included lateral restraints of the top flanges at the load and support points. These lateral restraints correspond with the position of the cross-frames in the test specimens. The cross-

frames prevented lateral movement of the top flanges by connecting the web just below the top flange to the bottom flange on the opposite side of the cross-section. These cross-frames consisted of angles and plates as described in Chapter 3. Since these frames were attached rigidly near the top flanges of the girder, they must bend if the top flanges are to warp during buckling. Thus the cross-frames add some warping restraint, as shown in Figure 5.6.

The effects of this warping restraint were investigated using the BASP half-girder model presented in Chapter 2. The stiffness of a cross-frame was estimated based on the frame member sizes and assuming the cross-frame was bent in double curvature (6EI/L stiffness). A stiffness of 130 k-in/rad was estimated. These restraints were modeled as rotational springs attached to the top flanges at all cross-frame locations and resulted in a 0.1% increase in the buckling load. Using a spring of infinite stiffness (i.e. full warping restraint) increased the buckling load only 5%. Therefore, the cross-frame warping restraint is not a significant factor in explaining the difference between tests and theory.

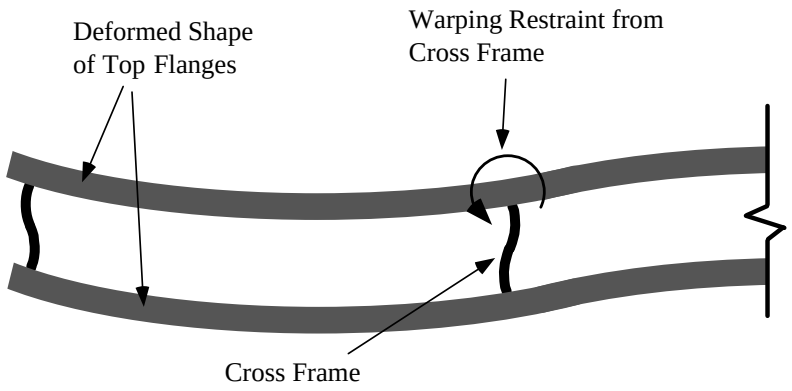


***Figure 5.6: Warping Restraint of Top Flanges Caused by Cross-Frames***

### 5.4.2 Web Separation

One dimension of the actual test specimen which was not modeled exactly was the distance between the webs. The finite element model consisted of webs which were separated a distance equal to the width of the bottom flange, 20.0 in.. The actual distance between the centerline of the webs was 18.5 in. since continuous welds were placed along the outside between the webs and bottom flange, as shown in Figure 5.7.

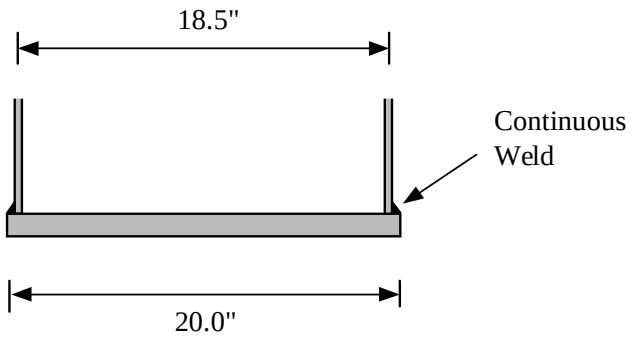


***Figure 5.7: Actual Distance Between Webs of U-girder Test Specimen***

Based on the half-girder model presented in Chapter 2, a decrease in the distance between webs increases the effective torsional spring stiffness of the bottom flange. Using a web separation of 18.5 in., the torsional spring stiffness was increased by 8.1% but resulted in just a 0.3% increase in the buckling load. The increase in load was much smaller than the increase in stiffness because the buckling capacity is limited mainly by cross-section distortion.

### 5.4.3 Support Restraint

The finite element model presented in Chapter 2 was simply supported with overhanging end spans. As described in Chapter 3, the simply supported

condition was approximated in the laboratory by using two wide-flange beams for the supports. These supports added some rotational restraint to the U-girder test specimen. To investigate the effects of these supports, they were added to the ABAQUS finite element model as plates with dimensions equal to the webs of the support beams. These plates were fixed rigidly at the base and attached to the U-girder at the top. Figure 5.8 shows the finite element model with the supports.

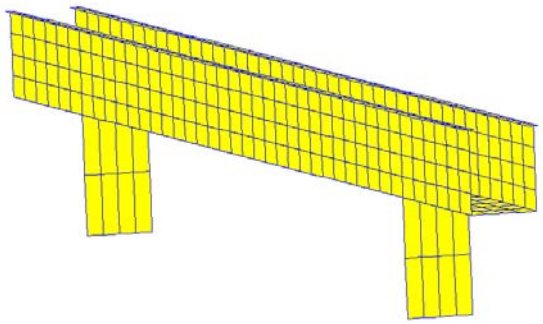

***Figure 5.8: Finite Element Model with Support Beams***

The ABAQUS eigenvalue analysis for the rectangular U-girder indicated a buckling load of 2714 k-in for the unstiffened U-girder with supports, an increase of 0.3% over the simply supported case. Large displacement analyses for the rectangular girder finite element model with supports also indicated almost no differences in behavior or buckling load.

### 5.4.4 Effective Web Height

The finite element analyses and hand calculations presented in Chapter 2 indicate that web distortion is significant in the buckling of U-girders. Reducing this distortion leads to notable increases in the buckling capacity. As mentioned above, the laboratory test specimens featured webs which were attached to the top

and bottom flanges with continuous welds. These welds added restraint to the webs over the 1/4 in. web height. Assuming distortion was prevented in the area of the welds, the height of the web that was free to bend was actually 1/2 in. less than the full web height, as shown in Figure 5.9. Also, the finite element model geometry is based on the centerlines of the flanges and webs. Thus the web of the finite element model actually extends from the center of the bottom flange to the center of the top flange. This added an additional 0.5625 in. to the model's web height.

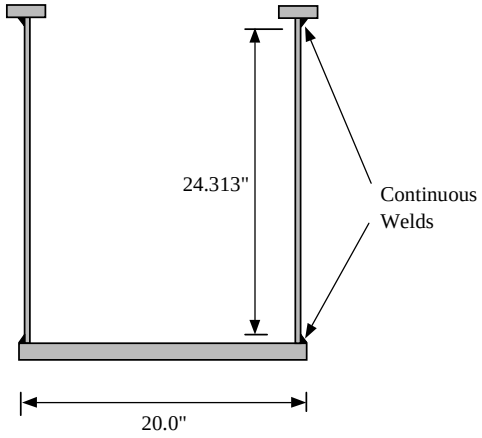


***Figure 5.9: Effective Web Height***

The sensitivity to web height was studied by reducing the rectangular girder's web height by 1 in.. The eigenvalue buckling load for this model was 2737 k-in, an increase of 1.2% over the original model's buckling load.

### 5.4.5 Web Imperfections

As discussed in Chapter 4, the top flanges of the U-girder test specimens were not perfectly straight. The large displacement analyses presented in section 5.2 indicated that the initial out-of-straightness of the top flanges had little effect

on the U-girder's buckling load. The webs of the test specimens also featured initial imperfections. These imperfections were not modeled in either the eigenvalue or large displacement analyses.

The imperfections of the rectangular girder's web were measured from a string line clamped to the web at both ends of the girder. The general shape and dimensions of these imperfections at the midheight of the web are shown in Figure 5.10.

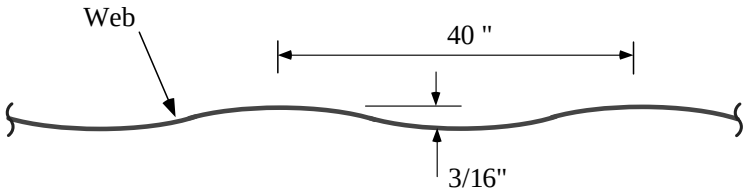


***Figure 5.10: Plan View of Typical Web Imperfections for Rectangular Girder***

The finite element analyses presented in Chapter 2 indicate that the buckling mode of an unstiffened U-shaped girder is characterized by large amounts of web distortion. An example of this web distortion is illustrated in Figure 2.14. These analyses also indicate that increasing the web's lateral stiffness leads to much higher buckling loads.

Previous research (Elgaaly,1995; Sherman,1971) has been conducted investigating the effects of "corrugated" webs for use in steel plate girders. The webs of these girders are folded to form a web which has a much larger lateral moment of inertia than a straight web of the same thickness. The imperfection shown in Figure 5.10 is similar to the shape of a corrugated web. The imperfect

web with a wave pattern has a larger lateral moment of inertia than the straight web of the finite element models.

A calculation was performed to estimate the effects of this web imperfection. The shape of the imperfection was approximated as a sine curve. A lateral moment of inertia was calculated based on the dimensions provided in Figure 5.10. The moment of inertia was determined to be 0.228 $in^4$, a 438% increase over a straight web with the same thickness. Thus a 0.25 in. thick web with this initial imperfection has the same stiffness as a 0.41 in. thick straight web. Increasing the thickness of the ABAQUS model's web to 0.41 in. gives a buckling load of 4907 k-in, an 81% increase over the original model's buckling load. This indicates that the web imperfections have a very significant effect on the buckling strength of the U-girder.

Based on this evaluation, it appears that the initial web distortion gives the web a greater out-of-plane stiffness. This explains why the experimental results are higher than the theoretical solutions, which were based on straight webs.

# CHAPTER 6

# Summary and Conclusions

## 6.1 SUMMARY

Trapezoidal box girder systems typically consist of twin steel U-shaped girders with a concrete deck acting compositely as the top flange. As previously discussed, the top flanges of these U-girders are susceptible to lateral-torsional buckling during transport, erection, and placement of the deck. There is no existing codified design method for lateral bracing of U-shaped girders. Minimizing the amount of bracing used will lead to a more efficient design since this bracing makes up a significant amount of the total costs and is not utilized once the concrete deck has cured.

In order to develop a design procedure for lateral bracing of U-girders, the behavior of unbraced U-shaped girders was first studied. An analytical program was undertaken to study the buckling behavior of unstiffened and transversely stiffened U-shaped girders using finite element models. A series of laboratory experiments were then performed using U-girder scale models in order to verify these analytical results. Finally, the analytical and experimental results were compared with existing design equations for torsionally braced I-shaped beams.

## 6.1 CONCLUSIONS FROM ANALYTICAL PROGRAM

The results of this study indicate that :

1. The behavior of a U-shaped girder can be approximated as two "half-girders" with continuous torsional bracing and bottom flange lateral restraint.
2. The stiffness of the torsional brace in a half-girder model depends upon the thickness and width of the U-girder's bottom flange. Increasing the brace stiffness results in a non-linear increase in the buckling capacity and a switch to higher buckling modes. Thus, the first buckling mode for a U-girder may be a multi-wave shape.
3. The buckling capacity of a U-girder can be severely limited by distortion of the web. This distortion can be controlled and the buckling capacity increased with the use of transverse stiffeners. For the U-girders studied, adding transverse stiffeners increased the buckling capacity by as much as 100%.
4. A U-shaped girder with a trapezoidal cross-section has a buckling capacity less than a rectangular girder of similar dimensions. This reduction can be attributed to lateral components of shear which occur in the sloping webs. The trapezoidal section had a buckling capacity 8.5% less than the rectangular section for the girders studied in this report.
5. Equations developed for singly-symmetric I-shaped beams with continuous torsional bracing predicted buckling capacities almost 60% higher than a finite element analysis. The cause of this discrepancy is the effective moment of inertia term $I_{eff}$, which was developed for $\rho$ values between 0.1 and 0.9. The value of $\rho$ for the girders studied was just 0.02.

Using the $I_{eff}$ equation for $\rho$ values outside these limits gave very unconservative results.

## 6.2 CONCLUSIONS FROM EXPERIMENTAL PROGRAM

The elastic buckling loads were determined using the Southwell plotting method and compared with finite element analyses. These comparisons showed that :

1. The Southwell buckling loads for the laboratory experiments were significantly higher than the finite element eigenvalue buckling loads. However, a series of large displacement finite element analyses simulating the laboratory tests indicated the Southwell method may not be accurate for cases where the deformed shape is not a sine wave. The deformed shape may vary from a sine wave because of the attached stiffeners and initial top flange imperfections.
2. The loads actually applied to the test specimens during the experiments exceeded the eigenvalue buckling loads by as much as 20%. Any increase in web stiffness can lead to dramatic increases in the buckling capacity since an unstiffened U-girder's buckling mode features large amounts of cross-section distortion. Web imperfections are the likely cause of the discrepancy between the finite element analyses and laboratory tests.

3. A series of large displacement finite element analyses indicated that small initial imperfections in the top flanges have little effect on the buckling load.
4. These large displacement analyses also indicate that U-shaped girders have some post-buckling strength at higher lateral displacements.

## 6.3 FUTURE RESEARCH

The results of the analytical study showed that the buckling behavior of a U-shaped girder could be estimated by considering the girder as two torsionally braced half-girders. The design equations developed for torsionally braced beams gave very unconservative results for these half-girders when compared to finite element and test results. The cause of the error is the $I_{eff}$ term, which was developed for values of $\rho$ for between 0.1 and 0.9. Further development of $I_{eff}$ for $\rho$ values outside of these limits is necessary for an accurate unbraced U-girder design equation. The effects of top lateral bracing systems can then be studied and minimum requirements developed.

The discrepancy between finite element buckling loads and the actual loads applied to the laboratory test specimens was attributed to the imperfections of the webs. The effects of the imperfections were estimated by measuring their shape and calculating an effective lateral stiffness of the web. A straight web with this increased stiffness was input into the finite element model by increasing the thickness of the web. The effects of these initial imperfections should be

further verified by performing a large displacement analysis including the measured web imperfections in the model geometry.

# APPENDIX A

## Test Data

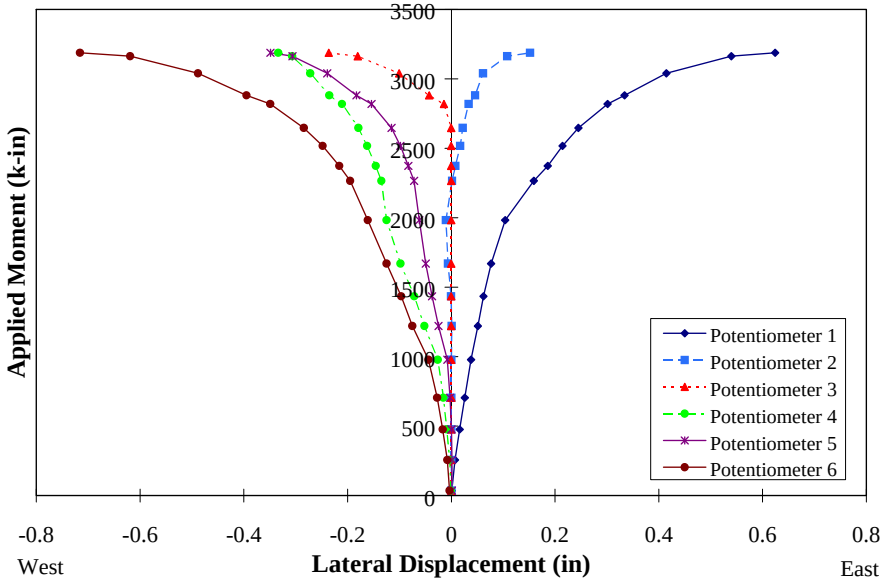


***Figure A.1: Lateral Displacement Reading for Test R1***

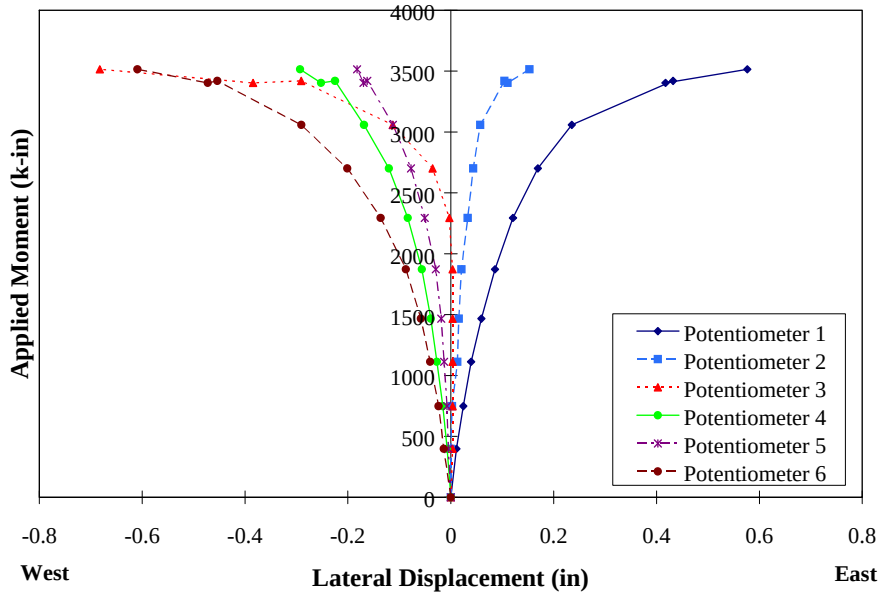


***Figure A.2: Lateral Displacement Readings for Test R2***

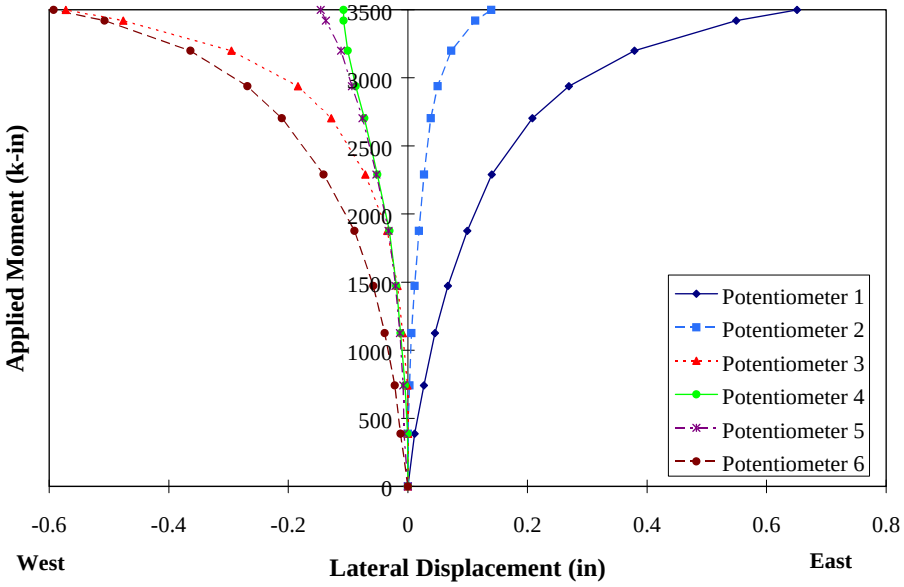


***Figure A.3: Lateral Displacement Reading for Test R3***

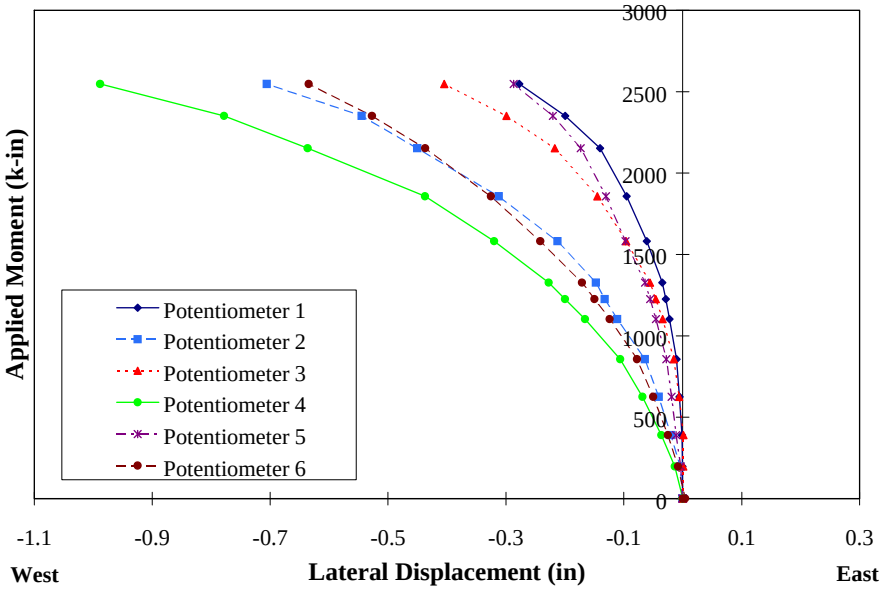


***Figure A.4: Lateral Displacement Readings for Test T1***

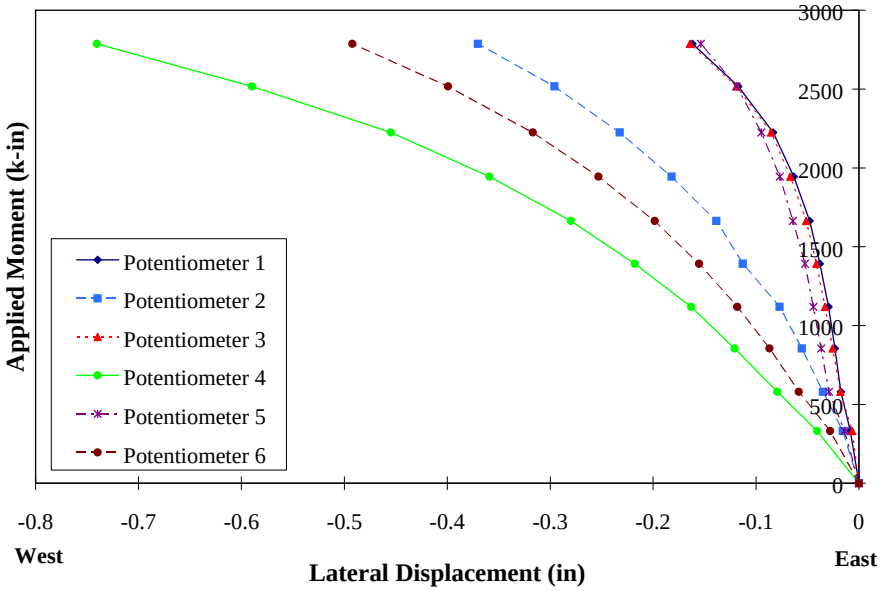


***Figure A.5: Lateral Displacement Readings for Test T2***

# References


Akay, H.U., Johnson, C.P., and Will, K.M., 1977, "Lateral and Local Buckling of Beams and Frames.", *Journal of the Structural Division*, ASCE, ST9, September, pp. 1821-1832.

Basler, K. and Kollbrunner, C.F., 1969, *Torsion in Structures*, Berlin: Springer-Verlag, pp. 14-15.

Choo, K.M., 1987, Thesis presented to The University of Texas at Austin, May, "Buckling Program BASP for Use on a Microcomputer."

Elgaaly, M., Seshradi, A., and Hamilton, R. "Shear Strength of Beams with Corrugated Webs." *Journal of Structural Engineering*, Apr., 1996, p.390.

Helwig, T.A., Yura, J.A., and Frank, K.H., 1993, "Bracing Forces in Diaphragms and Cross Frames", Structural Stability Research Council Conference, April 6-7, Milwaukee, WI.

Meck, H.R., 1977, "Experimental Evaluation of Lateral Buckling Loads.", *Journal of the Engineering Mechanics Division*, ASCE, EM2, April, pp. 331-337.

Sherman, Donald and Fisher, James, 1971, "Beams with Corrugated Webs." Proceedings, First Specialty Conference on Cold-Formed Steel Structures. Rolla: University of Missouri-Rolla, pp.198-204.

Southwell, R.V., 1932, "On the analysis of Experimental Observations in the Problems of Elastic Stability.", *Proceedings of the Royal Philosophical Society of London*, Series A, Vol. 135, April, p. 601.

Taylor, A.C., and Ojalvo, M., 1966, "Torsional Restraint of Lateral Buckling.", *Journal of the Structural Division*, ASCE, ST2, April, pp. 115-129.

Timoshenko, S., and Gere, J., 1961, *Theory of Elastic Stability*, New York: McGraw-Hill Book Company, pp. 190-191.

Trahair, Nicholas S., 1969, "Deformations of Geometrically Imperfect Beams.", *Journal of the Structural Division*, ASCE, ST7, July, pp. 1475-1496.

Winter, G., 1960, "Lateral Bracing of Columns and Beams," *ASCE Transactions*, Vol. 125, pp. 809-825.

Yura, Joseph A., 1993, "Fundamentals of Beam Bracing." Structural Stability Research Council Conference - Is Your Structure Suitably Braced?, April 6-7, Milwaukee, WI.